Calorimetry of the Charging of Porous Carbon Electrodes for Blue Energy

Bachelor thesis by Elian Griffioen

Supervised by Ben Erné

Evaluated by Ben Erné and René van Roij

18 July 2015

Van ’t Hoff Laboratory for Physical and Colloid Chemistry

Utrecht University

“L’échec est le fondement de la réussite.”- Lao Tseu

Abstract

Blue energy is the electrical energy extracted from the irreversible mixing of salt and fresh water. One way to obtain this energy is by charging porous carbon electrodes in salt water and discharging them in fresh water. During the charging and discharging of these electrodes temperature changes occur. Temperature increases during the charging step due to ion entropy loss and temperature decreases during the discharging step due to ion entropy win. A temperature controlled setup was built and calibrated to measure heat effects during charging and discharging. The temperature effects were separable into Joule heating and ion entropic heat effects. The ion entropic effects in agreement with the theoretical predictions, led to production of heat during the charging step and removal of heat during the discharging step. The experimental entropic heat effects were ten times weaker than predicted from Janssen et al. (PRL, 113, 268501, 2014). A key difference between experiments and theory is that only a small fraction of the pore volume consists of electrical double layers instead of the assumed total pore volume. Further research is welcome on the influence of electrolyte concentration and temperature on the entropic heat effects.

Table of Contents

1. Introduction

Blue energy is a hot topic nowadays. In short it is the electrical energy which can be extracted from the irreversible mixing of salty sea and fresh river water. The capacitive mixing method is a way to acquire this energy. This method uses porous carbon electrodes to serve as an electrical double layer capacitor which can be charged and discharged. An electrical double layer arises upon charging in salt water, which is then replaced by fresh water. In this step the electrical double layer potential increases. The electrodes are discharged in fresh water and afterwards fresh water is replaced by salt water. The area of this cycle based on charge and potential corresponds to the maximal amount of work that can be extracted from this cycle [1].

In an adiabatic system (which means no heat exchange with the environment) the charging and discharging steps are accompanied with temperature changes. This is partly due to the ion entropy loss during the charging step and ion entropy win during the discharging step [2]. During charging, the ion entropy decreases, which is compensated by a water entropy increase and consequently a water temperature increase. This process is reversed during discharging. The size of these effects are estimated up to a few Kelvin [2]. These effects are fundamentally interesting due to the thermodynamic behaviour of ions in charging and discharging of porous electrodes. Moreover, this is technologically relevant since temperature can have a significant influence on the cycle efficiency of capacitive mixing devices [2] and since temperature influences the degradation of porous electrodes [3]. Another heat effect upon charging and discharging is Joule heating: the heat that is produced by current flow through a resistance [3]. So two heat effects are present during charging and discharging steps in the capacitive mixing cycle.

These theoretically predicted ion entropy effects on temperature have not yet been found experimentally. In this bachelor thesis these entropic effects upon charging and discharging are studied experimentally. The objective is to measure entropic effects and to compare the results to the theoretical predictions. At the Physical and Colloid Chemistry group no research has yet been done on blue energy systems. An experimental blue energy study is relatively new for us, so the research started with becoming familiar with the system and experimental methods. This is done by trying to reproduce steps of the cycle and to reproduce the theoretically described influence of temperature on cycle steps. Subsequently, the entropic effects are measured in a temperature controlled system. First, this system is calibrated using heating elements which produce a controlled amount of Joule heat. Then, the heat effects of the charging and discharging steps are measured and separated into Joule and entropic heat effects. Finally, the results are compared to the theoretical predictions.

2. Theory

2.1 Blue energy and the capacitive mixing method

Blue energy is the electrical energy acquired by making use of the salinity difference between salty sea water and fresh river water [4]. The energy comes from irreversible mixing of salty seawater and fresh river water. For every liter of river water which is mixed with sea water, 2.2 kJ can be acquired [5]. If all places where rivers and sea meet are utilized, the demand for energy worldwide will be filled for 20 percent [4]. In the Netherlands, a country with many rivers and seas, a commercial plant has already been built [6]. To get energy from the salinity difference between sea and river water, different methods are possible [7]. The process can be reversed as well: use energy to desalinate salt water. This is very useful because of the water scarcity in the world. Because both are opposite processes, the same methods can be used [8]. Membrane based methods are very common, especially pressure-retarded osmosis (PRO) and reverse-electrodialysis (RED) for harvesting energy purposes [9]. In pressure-retarded osmosis, a membrane separates the two solutions and the osmosis is converted into electrical energy. In reverse-electrodialysis, an ion-selective membrane is used to separate the solutions and the cations and anions migrate to different electrodes. This is converted into a current by redox reactions [9]. However, upscaling is difficult because the large membranes are not yet cost-efficient [8-10].

In 2009 a new method was stated by Brogioli in which electrical energy can be acquired without membranes [1]. This is called the capacitive energy extraction from double layer expansion technique (CDLE) or simply the capacitive mixing method [1,11]. The method is based on two charged electrodes which are immersed in alternately salt and fresh water. In this way the system is a capacitor in which the electrolyte solution (salt or fresh water) serves as a dielectric medium [1,11]. The electrodes are made of activated carbon, which is very porous. This has many advantages. Activated carbon has a high surface area (1,000 - 2,000 m^2/g) and therefore much more charge can be stored compared to conventional solid-state capacitors. Capacitances of 5-20 $\mu F/cm^2$ are found for activated carbon, so the electrodes have a high capacitance due to the huge surface area. However, they have a lower energy density than batteries: the amount of energy per kilogram is less which means that for high energy purposes a fast discharge is needed [12]. The double layer capacitance of porous electrodes can be described with the following formula

$$C = \frac{\epsilon_0 \epsilon_r A}{d} \quad (1)$$

in which ϵ_0 is the permittivity of vacuum, ϵ_r the relative permittivity of the electrolyte, A the surface area of the electrode and d the effective thickness of the electrical double layer [12].

2.2 The electrical double layer in porous electrodes

If an electrode is charged in a electrolyte solution, ions are attracted to the electrodes and an electrical double layer of ions will be formed which can be seen in Figure 1. This electrical double layer can be described with the Gouy-Chapman theory [13-15]. The double layer consists of two layers: a Stern layer and a diffusion layer. The Stern layer consists of absorbed ions or solvent molecules. The diffusion layer consists of ions which are in an equilibrium of the electrostatic interactions (which attract the ions to the electrodes) and diffusion (which tends to a homogeneous solution) [1,15]. The thickness of the double layer is on the order of the Debye length [11].

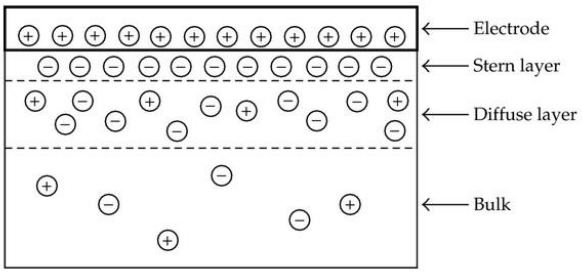

Figure 1. An electrical doube layer consisting of a Stern layer and diffuse layer formed at a flat electrode. Reproduced from [21] (Copyright ISRN Applied Mathematics 2012)

The Debye length is a measure of the reach of a charge carrier's electrostatic effects. In other words, it can be interpreted as the maximum length at which a charge carrier has any electrostatic interactions with other ions. It can be described with the following formula for monovalent electrolyte solutions [16]

$$\kappa^{-1} = \sqrt{\frac{\epsilon_0 \epsilon_r k_B \mathrm{T}}{2e^2 n_0}} \tag{2}$$

in which the Debye length is inversely proportional to the square root of the electrolyte concentration. The thickness of the electrical double layer is on the order of the Debye length, which means that a thicker electrical double layer is formed at lower electrolyte concentrations. After a change from salt to fresh water, ions diffuse away from the electrodes (against the electrostatic interactions) so the potential difference increases.

Combining the Poisson-Boltzmann equation with this Gouy-Chapman model, gives an expression for the electrical double layer potential difference between electrodes and the bulk solution[1,15]:

$$\psi = \frac{2k_B \mathrm{T}}{e} \sinh^{-1} \frac{\sigma}{\sqrt{8cN_A \epsilon_0 \epsilon_r k_B \mathrm{T}}} \tag{3}$$

This formula shows again the concentration dependence of the electrical double layer potential. However, the formula is quantitative for flat electrodes, but only qualitative for porous electrodes. The formula is quantitative for pores that are bigger than the electrical double layer thickness, but is not quantitative for pores smaller than this thickness [1]. In Figure 2, a distribution of ions in a porous carbon electrode is shown.

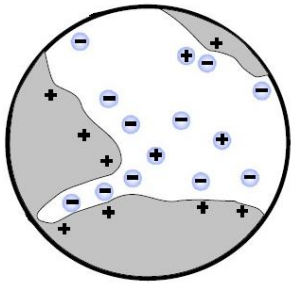

Figure 2. A distribution of ions in a porous electrode. Reproduced from [2] (Copyright Physical Review Letters 2014)

Box 1. Explanation of variables in formulas

k_B = Boltzmann constant (J/K)

T = temperature (K)

e = positive elementary charge (C)

σ = surface charge density ($\mathrm{C/m^2}$)

c = concentration ($\mathrm{mol/m^3}$)

N_A = Avogadro constant ($\mathrm{mol^{-1}}$)

ϵ_0 = dielectric permittivity of vacuum ($\mathrm{CV^{-1}m^{-1}}$)

ϵ_r = relative permittivity of the electrolyte

n_0 = concentration ($\mathrm{m^{-3}}$)

2.3 The capacitive mixing cycle

So the potential difference can be influenced by alternating solutions of low and high concentrations (river and sea water). In this way, the work of alternating solutions can be converted into electrical work. The capacitive mixing method is based on this principle. To extract energy from the salinity difference, a cycle is used which consists of four steps [1,10]. It is shown in Figure 3:

AB The electrodes immersed in sea water are charged from Q_A to a higher charge Q_B.

BC The sea water is replaced by river water; as a consequence the potential difference increases from ψ_B *to* ψ_C.

CD The electrodes immersed in river water are discharged from Q_B to a lower charge Q_A.

DA The river water is replaced by sea water; as a consequence the potential difference decreases from ψ_D *to* ψ_A.

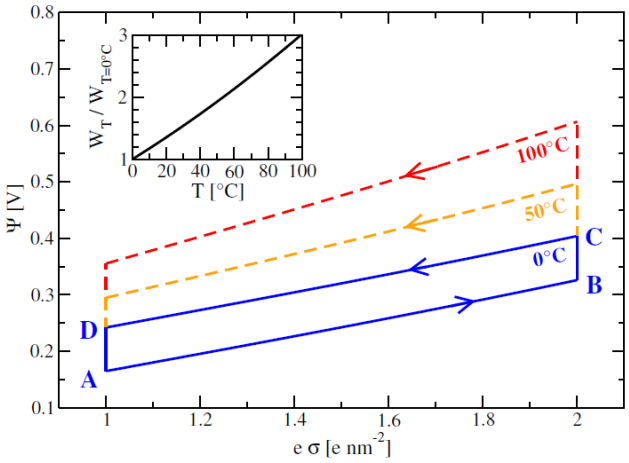

Figure 3. Cycles at different temperatures of fresh water.
Reproduced from [2] (Copyright Physical Review Letters 2014)

In the charging and discharging steps (AB and CD) current flows through the electrical circuit and this current can be used as electrical energy. In this way, electrical energy is extracted from the cycle and the energy that can be extracted from the cycle is higher than the energy it costs [1]. The cycle has many parallels with the Carnot Cycle, but this cycle based on potential and charge instead of pressure and volume. The (maximal) amount of work by the system is equal to the area of the cycle [10]:

$$W = -\oint \psi dQ \tag{4}$$

The efficiency of the Carnot cycle depends on the temperatures T_H and T_L of the heat reservoirs and analog to this the efficiency of the capacitive mixing cycle depends on the chemical potentials of the salt and fresh water. So for an efficient cycle, a solution with a high (sea water) and low chemical potential (river water) is needed [10].

Theoretical calculations show that the temperature of fresh water has a big influence on the work of the cycle [2]. This can be seen in Figure 3, which shows different cycles with different temperatures of fresh water. From Equation 3 can be seen that potential increases upon increasing temperatures (at constant charge). If the charging step in salt water is performed at 0 ˚C, but the discharging step

in fresh water at higher temperatures, the area and consequently the work of a cycle increases. This has a big influence, since the amount of work using 100 ˚C fresh water is three times higher than the amount of work using 0 ˚C fresh water. A possible application is using warm waste water from factories for instance as fresh water source. In this way, waste water can be useful to enhance the work of these cycles [2].

2.4 Entropic temperature effects

An interesting theoretical prediction has been done about the charging and discharging step in an adiabatic system [2]. In an adiabatic system, there is no heat exchange with the surroundings of that system [16]. Temperature changes occur in the charging and discharging step due to loss and win of ion entropy respectively. If the electrodes are charged, more ions are attracted to the electrodes, so there is less freedom of movement for the ions and the ion entropy decreases. It is an adiabatic system, so the loss in entropy must be compensated. This is done by increasing the water entropy and as a consequence the temperature rises. The inverse process occurs during the discharging step: ions return to the bulk solution and gain more entropy which is compensated by a water entropy loss. Consequently, the temperature decreases. A quantitative expression can be derived from the adiabatic condition dS (Q,T)=0. A complete derivation is shown in Appendix A. The formula for this entropic temperature effect is as follows

$$dT = -\left(\frac{dS}{dT}\right)_Q^{-1}\left(\frac{dS}{dQ}\right)_T dQ = \frac{2T}{c_Q L}\left(\frac{d\psi}{dT}\right)_Q e d\sigma = \frac{2T}{c_Q V_{EDL}}\left(\frac{d\psi}{dT}\right)_Q dQ \quad (5)$$

in which Q is the charge, T the temperature, c_Q the specific heat capacity of the solution, L the pore size, Ψ the electrical double layer potential, e the positive elementary charge, σ the surface charge density and V_{EDL} the volume of the electrical double layer. This volume is assumed to be equal to the pore volume of the electrodes. The size of the effects is influenced by the temperature of the solution, the pore size and likewise the pore volume and the amount of charge on the electrodes. The effect is estimated in both steps at a few degrees Celsius depending on the chosen experimental conditions [2]. Despite the size of the effect, it still has an influence on the work of the cycle and especially if the cycles are optimised in industry [2]. Moreover, temperature of electrodes influences the lifetime of carbon electrodes. The degradation is accelerated at higher temperatures: for every 10 ˚C above 25 ˚C the lifetime is halved. The influence of the entropic temperature effect on degradation of porous electrodes is important, for instance in engineering of this electrodes [17,18].

2.5 Joule heat effects

Two types of heating occur during charging and discharging steps. To explain heat effects in a clear way and to prevent misunderstandings, produced heat by the system is defined as positive and removed heat from the system is defined as negative. In addition to entropic heating, Joule heating takes place as well [3]. Joule heating is the heat that is produced if a current flows through a resistance. An expression for this type of heating is

$$\int I^2 R dt = \int IV dt \quad (6)$$

in which I is the current, R the resistance through which current flows and V the potential over the resistance. Contrary to entropic heating, which is reversible, Joule heating is irreversible. In both steps (charging and discharging) the produced heat is positive [3]. Joule heating is produced by the current flow through the resistance of the pores and the solution [3]. A typical electrical circuit for an

electrical double layer capacitor with porous electrodes is shown in Figure 4. Firstly an electrical double layer capacitor is placed in this circuit. However, the capacitor has problems with charge leakage due to self-discharge [19]. Therefore a leakage resistance in parallel across the capacitors is added to the circuit [19,20]. To complete this circuit, it is modified by adding a pore resistance, which is the resistance of the electrolyte in the pores, and a resistance of the electrolyte solution between the electrodes [3,20]. Theoretically, in porous electrodes there is a distribution of double layer capacitors and pore resistance over the whole electrode due to its irregular geometry [3,20]. Since this is beyond the purpose of this research, it is simplified in a general capacitor and pore resistance.

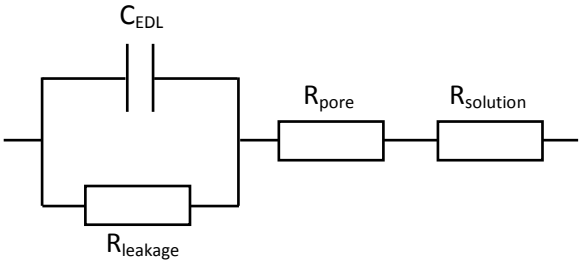

Figure 4. An electrical circuit for an electrical double layer capacitor with porous electrodes.

To calculate the Joule heating current and either voltage or resistance has to be known. The resistance of the solution can be estimated, but the resistance of the pores is difficult to know due to the irregularity of the pores. Therefore using voltage and current for Joule heating is easier. If a voltage V_{max} is applied, it is distributed among the electrical double layer and the resistance. To simplify, the sum of the pore and solution resistance is called solution resistance (R_{sol}). If an electrical double layer is formed, the potential across this layer increases upon formation. This is reversed in deformation of the double layer. Plots of the potential distribution in the charging and discharging step are shown in Figure 5:

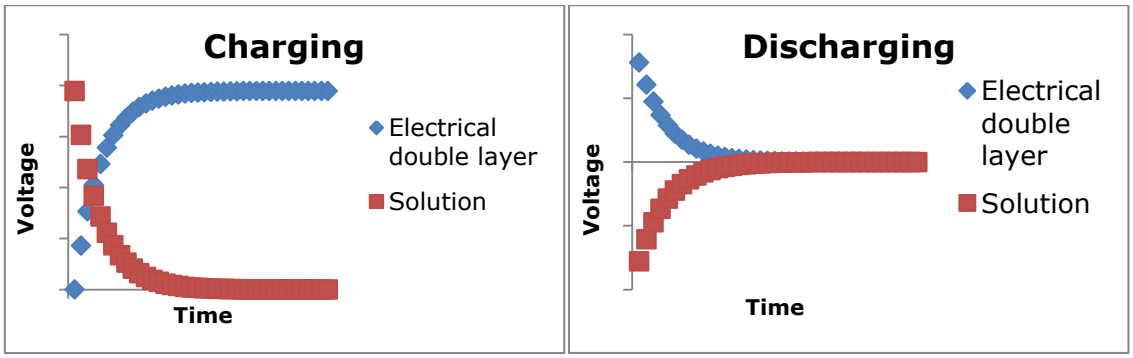

Figure 5. Potentials of the electrical double layer and solution in time for the charging and discharging step.

- Charging: At first, the total voltage is solely distributed among the solution. During charging, the double layer is formed and the potential difference across this layer increases. Similarly, the potential difference across the solution increases. The rate of charging is influenced by the current as a function of time.

$$V_{EDL} = V_{max}\frac{\int_0^t Idt}{\int_0^\infty Idt}, V_{sol} = V_{max}(1 - \frac{\int_0^t Idt}{\int_0^\infty Idt}) \quad (7)$$

- Discharging: In this step, the applied voltage is 0 Volt. Initially, the electrical double layer still has a potential difference of 1 V, so the potential difference across the solution is -1 V. During the discharging step, both potentials end at 0 V. The rate of discharging again depends on the current as a function of time.

$$V_{EDL} = V_{max}\left(1 - \frac{\int_0^t Idt}{\int_0^\infty Idt}\right), V_{sol} = -V_{max}(1 - \frac{\int_0^t Idt}{\int_0^\infty Idt}) \quad (8)$$

In these formulas, V_{max} is the applied voltage in the charging step, V_{EDL} the voltage across the double layer, V_{sol} the voltage across R_{sol}, I the current, t the time and $\int_0^\infty \mathrm{Idt}$ the integral of the current over the whole charging or discharging step. With this expression of V_{sol} which only depends on current and time, the Joule heating can be calculated by only measuring current in time.

3. Experimental methods

The experimental research in this project has been divided into two parts: the pre-research and the cell measurements. In the pre-research many experiments were done to become familiar with the capacitive mixing method and to discover the best way to measure several aspects of the method. The measurements with the cell started when this cell was engineered by the glassblowers. Since both parts are totally different, I will split experimental methods in two sections.

3.1 Pre-research

3.1.1 Chemicals

In this part, two solutions are used. For salty sea water, a sodium chloride solution of 0.6 M has been used. For fresh river water, a sodium chloride solution of 0.02 M has been used. The 0.6 M NaCl solution was prepared by dissolving 7.01 g NaCl in 200 mL of milli-Q water in a laboratory bottle with a volume over 200 mL. The 0.02 M NaCl solution was prepared by dissolving 0.23 g NaCl in 200 mL of milli-Q water in a laboratory bottle with a volume over 200 mL.

Activated carbon was used for electrodes. Electrodes were cut from a sheet of layers of activated carbon. The thickness was 0.5 mm and other properties were a mass density of 0.58 g/mL, a porosity of 65 % and a BET-area of 1330 m_2/g [11].

Graphite rods were used to conduct currents and voltages to electrodes. The rods had a diameter of 3 mm. Graphite from a graphite sheet (thickness 0.2 mm) was incorporated in the clamp. Graphite is non-porous.

3.1.2 Setup

The first setup was a simplified one in a petri dish. It is shown in Figure 6. Electrodes of 4 x 4 mm were cut from the activated carbon sheet and placed in the petri dish. On this electrodes graphite rods were placed which are fixed in clamps on a tripod. Via crocodile clips on the graphite rods and jumper cables the electrodes are connected to a potentiostat/galvanostat. The electrodes are immersed in a solution by filling the petri dish.

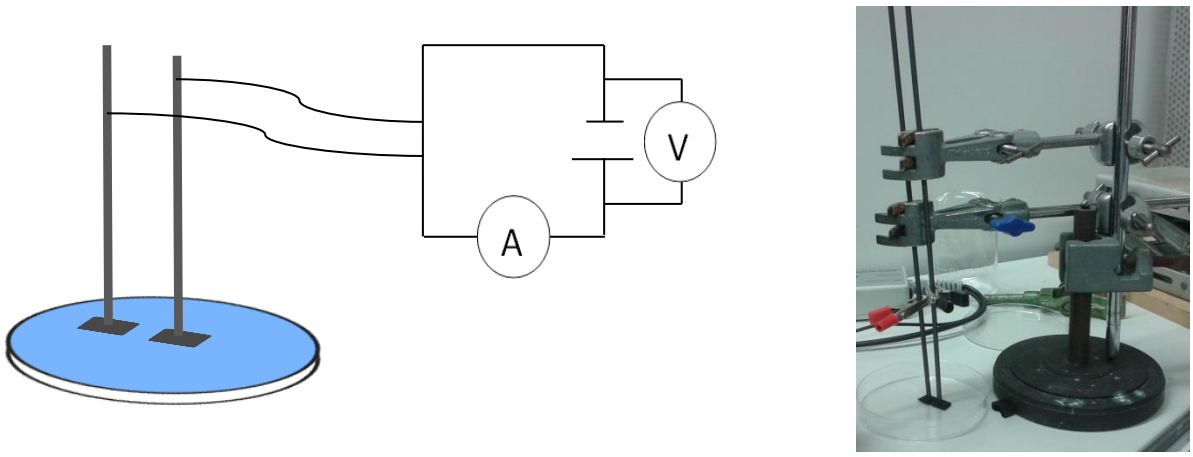

Figure 6. (Left) Schematic drawing of the setup. (Right) Picture of the setup.

A more advanced setup was a clamp in which the electrodes can be placed separated by a spacer. The clamp has been made of two plastic bars which are connected by two screws at one end of the bars. Next to these screws is another screw with which the distance between the other end of the bars can be tuned. Graphite foil from the graphite sheet has been glued on the surface of the bars. Connected to these bars and to the graphite foil are two screws and copper wire has been wrapped around this screw. At the end of the clamp two electrodes of 4x4 mm are placed with a paper (thickness 0.125 mm) between them which serves as a spacer. The copper wires can be connected to Autolab via crocodile clips and jumper cables. The clamp is fixed in a beaker which is filled with NaCl solution. To measure at different temperatures, the beaker and clamp can be placed on a heating plate. This heating plate has a temperature probe to monitor the temperature and to regulate the added heat to precisely tune the temperature. A schematic drawing of the clamp is shown in Figure 7 together with pictures of the setup with and without a heating plate.

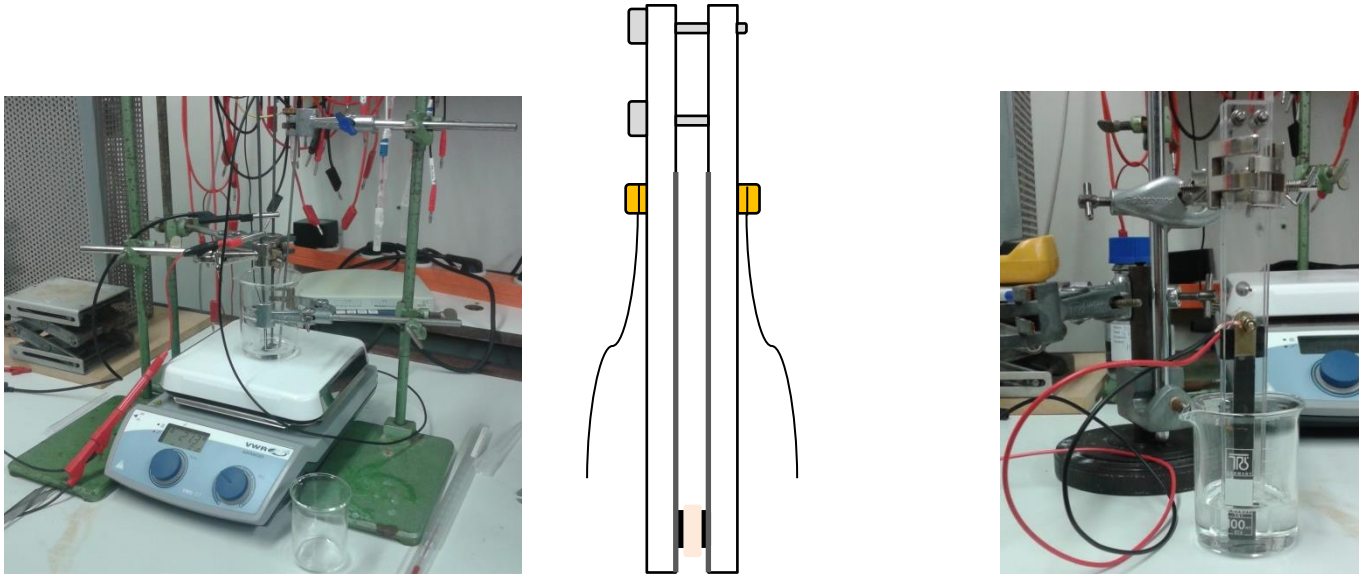

Figure 7. (Left) Setup with the clamp on a heating plate . (Middle) Schematic drawing of the clamp with two electrodes separated by a spacer (paper). (Right) Setup with the clamp in a beaker for room temperature measurements.

For applying currents and voltages a potentiostat/galvanostat was used: PGSTAT100 from the company Metrohm Autolab B.V. The used software was NOVA 1.10.3. The procedures used are:

- Chrono potentiometry: applying a constant current and measuring voltage and current
- Chrono amperometry: applying a constant voltage and measuring current and voltage

3.1.3 Measurements

Temperature dependence of charging and discharging steps with constant current

The electrical double layer potential at a certain surface charge density is theoretically higher at higher temperatures of fresh and salt water [2]. To test if our setup works, this has been tested experimentally.

As setup, the clamp in beaker on the heating plate was used. Electrodes of 4x4 mm with a paper spacer (fold for one time, so thickness is 0.25 mm) were placed in the clamp and the clamp was immersed in 30 mL 0.02 M NaCl solution. Measurements were done at room temperature (25 ˚C) and higher temperatures varying from 50 till 80 ˚C. At temperatures higher than room temperature, a magnetic stir bar was used to obtain a homogeneous distribution of temperature in the solution. Measurements were done in a constant current mode. At first, potential was measured without current. Afterwards, potential was measured at an applied constant current. Finally, potential was measured without current. The procedure was as follows:

Chrono potentiometry (Δt > 1 ms)	
Set current	0.000 A
Wait time	5 s
Records signals (> 1 ms) galvanostatic	30 s
Interval time	0.01 s
Set current	5.000 x 10^{-5} A
Records signals (> 1 ms) galvanostatic	120 s
Interval time	0.01 s
Set current	0.000 A
Records signals (> 1 ms) galvanostatic	120 s
Interval time	0.01 s

Temperature dependence of charging and discharging steps with constant voltage

Again, the temperature dependence of the potential has been tested, but now measurements were done in the constant voltage mode. As setup, the clamp in beaker on the heating plate was used. Electrodes of 4x4 mm with a paper spacer (fold for one time, so thickness is 0.25 mm) were placed in the clamp and the clamp was immersed in 30 mL 0.02 M NaCl solution. Measurements were done at room temperature (25 ˚C) and at 67 ˚C. At temperatures higher than room temperature, a magnetic stir bar was used to obtain a homogeneous distribution of temperature in the solution. First a potential was measured, then a potential was applied 300 mV higher than the measured potential before and finally the potential was measured again. The procedure was as follows:

Chrono potentiometry (Δt > 1 ms)	25 ˚C	67 ˚C
Set current	0.000 A	0.000 A
Wait time	0 s	0 s
Records signals (> 1 ms) galvanostatic	30 s	30 s
Interval time	0.01 s	0.01 s
Chrono amperometry (Δt > 1 ms)		
Set potential	0.617 V	0.738 V
Records signals (> 1 ms) potentiostatic	700 s	700 s
Interval time	0.01 s	0.01 s
Set current	0.000 A	0.000 A
Records signals (> 1 ms) galvanostatic	30 s	30 s
Interval time	0.01 s	0.01 s

Effective surface area of porous carbon electrodes

Due to its porosity carbon electrodes have much more surface area compared to graphite (which is non-porous). The question is which part of this additional surface area is used for electrical double layer formation. In other words, what is the effective surface area of porous carbon electrodes. By measuring the capacitance per m^2, an expression for the effective surface area can be acquired.

- Porous electrodes: The setup with the clamp in a beaker was used. Electrodes of 4x4 mm with a paper spacer (fold for one time, so thickness is 0.25 mm) were placed in the clamp and the clamp was immersed in 30 mL 0.02 M NaCl solution.
- Graphite: The setup with the clamp in a beaker was used. Nothing was placed in the clamp so that only the graphite capacitance was measured. The clamp was immersed in 30 mL 0.02 M NaCl solution and the clamp was 1.7 cm below the meniscus of the solution.

Both measurements are performed by applying a constant current. The procedure was as follows:

Chrono potentiometry (Δt > 1 ms)	Graphite	Porous electrodes
Set current	0.000 A	0.000 A
Wait time	5 s	5 s
Records signals (> 1 ms) galvanostatic	30 s	30 s
Interval time	0.01 s	0.01 s
Set current	5.000×10^{-4} A	5.000×10^{-5} A
Records signals (> 1 ms) galvanostatic	170 s	330 s
Interval time	0.01 s	0.01 s

3.2 Cell measurements

3.2.1 Chemicals

In this part, four NaCl solutions with different concentrations were used: 1 mM, 10 mM, 0.1 M and 1 M. The solutions were prepared by dissolving the following amounts of sodium chloride in 200 mL of milli-Q water in a laboratory bottle with a volume over 200 mL:

Table 1. Amounts of added sodium chloride for preparating of different concentrations of NaCl solutions.

Concentrations (mole/Liter)	Added sodium chloride (g)
0.001	0,01168
0.01	0,1168
0.1	1,168
1	11,68

Activated carbon was used for electrodes. Electrodes were cut from a sheet of layers of activated carbon. The have a diameter of 25 mm. The thickness was 0.5 mm and other properties were a mass density of 0.58 g/mL, a porosity of 65 % and a BET-area of 1330 m_2/g [11].

Graphite disc are used as a support for the porous electrodes from activated carbon. These discs have a diameter of 25 mm and a thickness of 0.2 mm and are ordered at Sigma Aldrich.

3.2.2 Setup

These measurements were done in a temperature-controlled system: a thermostat bath. The used thermostat bath was Julabo F25. The used fluid in this bath was water. In this thermostat bath a cell was placed which was sealed from the environment. In this way the temperature in the cell was controlled by the thermostat bath which gave a temperature-controlled system. The cell was engineered in a way that two electrodes are close to each other with a temperature probe between them. The cell was fixed in a lid which was placed on top of the thermostat bath to seal it from the environment. The cell was connected to a potentiostat/galvanostat (PGSTAT100) via current wires. The used software for PGSTAT100 was Nova 1.10.3. Two Pt100 temperature probes were used. One of them was fixed in the cell between the electrodes (diameter of 0.5 mm, length of 200 mm), the other one was placed in the thermostat bath. In this way the temperature effects in the cell can be measured and the fluctuations of the thermostat bath are monitored. The hardware to convert the signals of the probes into a temperature value is PT104, a Pt100 data logger with a resolution of 0.001 K. The used software for measuring temperature was Picolog for Windows 5.24.2. These temperature probes are resistance thermometers made of platinum. The resistance of platinum depends on temperature. By measuring the resistance and converting this, a precise temperature can be acquired [22]. A schematic drawing of this setup is shown in Figure 8.

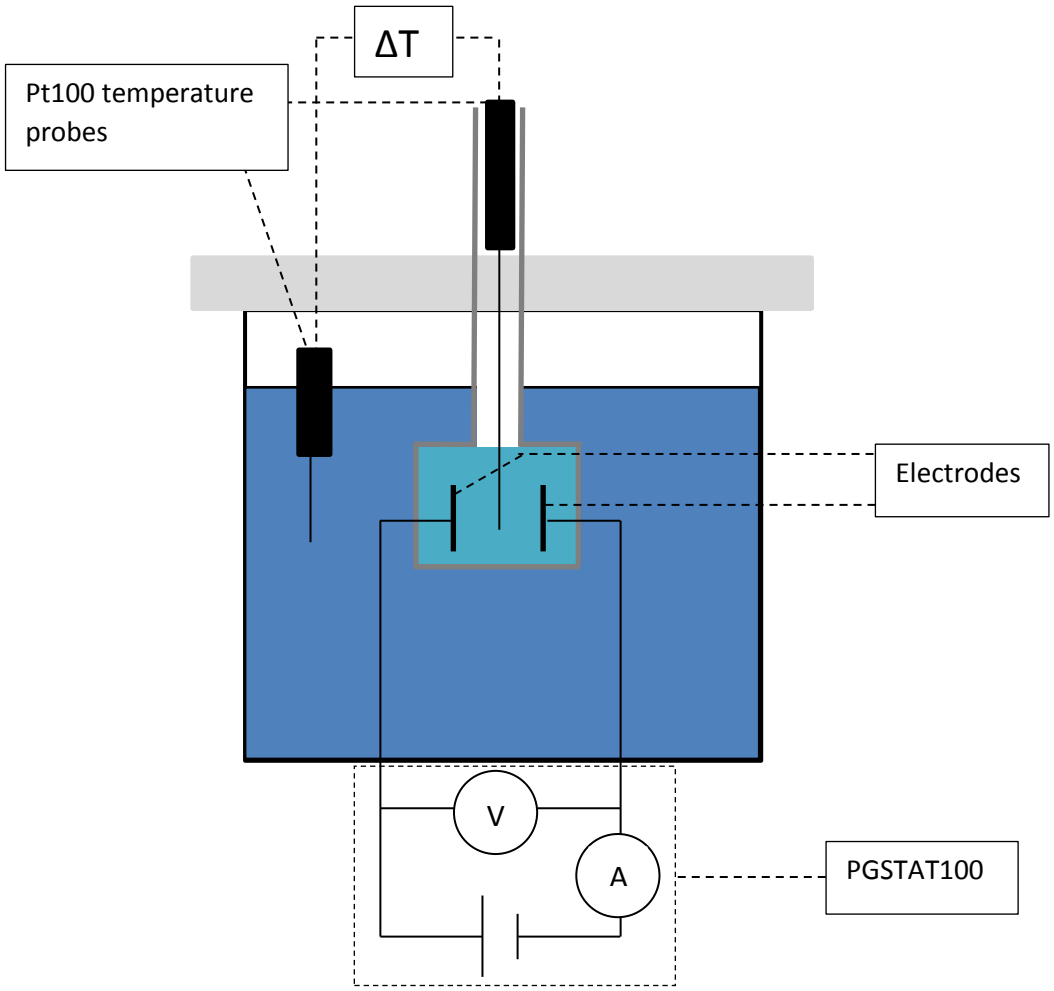

Figure 8. Schematic drawing of the setup: a cell in a thermostatbath; an electrical circuit with potentiostat/galvanostat, amperometer and voltmeter; two Pt100 temperature probes.

The cell consists of two glass plates in which an electrode (diameter of 25 mm) was placed and a third glass plate which between them separated by teflon spacers. This third glass plate has a hole with precisely the size of the electrodes and has a Pt100 temperature probe fixed between the two electrodes. In this way, the electrodes are separated by a distance of 2.11 mm. On the cell are connections for soft silicone tubes from the injection syringes (which are outside the thermostat bath). The whole cell is fixed in a lid which is placed on the thermostat bath. A pictures of the cell is shown in Figure 9. The precise dimensions of the cell can be found in Appendix B.

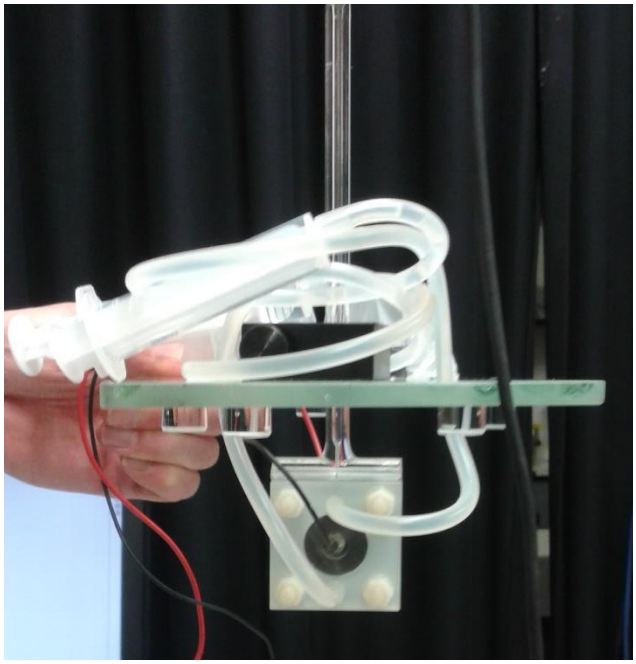

Figure 9. Picture of the cell with porous electrodes connected via soft silicone tubes to injection syringes. The cell is fixed in a lid that fits the thermostat bath.

For the calibration of the system, resistance wire is used. This is a metal wire with a known resistance. A controlled amount of Joule heating can be produced by applying a certain current. The resistance wire of 422 Ω. It is glued to a glass disc with a diameter of 25 mm (thickness is 3 mm). In the middle of the glass discs is a hole of 6 mm through which a current wire is glued to the resistance wire. These heating elements can be placed in the cell.

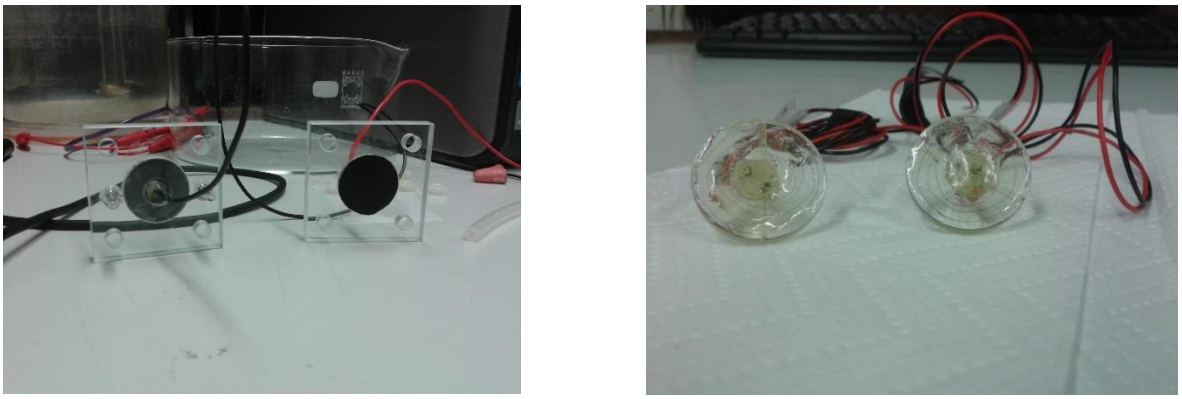

Figure 10. (Left) Porous carbon electrodes fixed in the glass plates of the cell. (Right) Heating elements.

After the calibration, porous electrodes are used. These electrodes are constructed on a glass discs (diameter of 25 mm, thickness of 3 mm) with a hole of 6 mm in the middle. A graphite disc (diameter of 25 mm, thickness of 0.2 mm) was glued on this disc. On this disc an activated carbon disk (diameter of 25 mm, thickness of 0.5 mm) was glued with conducting silver epoxy glue. Through the hole in the glass disc a current wire was glued to the graphite disc with silver expoy glue. These porous electrodes and the heating elements are shown in Figure 10.

3.2.3 Calibration

Heating elements are used in the calibration. These elements are connected the PGSTAT100 and the temperature in the cell was measured. The second temperature in the thermostat bath wasn't used. The following current are applied sequentially: 10, 8, 6, 4, 2, 1 and 0.5 mA. This was done for 400, 50 and 25 seconds with 400 seconds of zero current between each step. This whole procedure was performed in a cell with air (the empty cell) and a cell with milli-Q water. The following procedure was entered in PGSTAT100:

Chrono potentiometry (Δt > 1 ms)	Serie 1	Serie 2	Serie 3
Set current	0.010 A	0.010 A	0.010 A
Wait time	0 s	0 s	0 s
Records signals (> 1 ms) galvanostatic	400 s	50 s	25 s
Interval time	0.1 s	0.1 s	0.1 s
Set current	0.000 A	0.000 A	0.000 A
Records signals (> 1 ms) galvanostatic	400 s	4000 s	400 s
Interval time	0.1 s	0.1 s	0.1 s
Set current	0.008 A	0.008 A	0.008 A
Records signals (> 1 ms) galvanostatic	400 s	50 s	25 s
Interval time	0.1 s	0.1 s	0.1 s
Set current	0.000 A	0.000 A	0.000 A
Records signals (> 1 ms) galvanostatic	400 s	400 s	400 s
Interval time	0.1 s	0.1 s	0.1 s
Set current	0.006 A	0.006 A	0.006 A
Records signals (> 1 ms) galvanostatic	400 s	50 s	25 s
Interval time	0.1 s	0.1 s	0.1 s
Set current	0.000 A	0.000 A	0.000 A
Records signals (> 1 ms) galvanostatic	400 s	400 s	400 s
Interval time	0.1 s	0.1 s	0.1 s
Set current	0.004 A	0.004 A	0.004 A
Wait time	0 s	0 s	0 s
Records signals (> 1 ms) galvanostatic	400 s	50 s	25 s
Interval time	0.1 s	0.1 s	0.1 s
Set current	0.000 A	0.000 A	0.000 A
Records signals (> 1 ms) galvanostatic	400 s	400 s	400 s

Interval time	0.1 s	0.1 s	0.1 s
Set current	0.002 A	0.002 A	0.002 A
Records signals (> 1 ms) galvanostatic	400 s	50 s	25 s
Interval time	0.1 s	0.1 s	0.1 s
Set current	0.000 A	0.000 A	0.000 A
Records signals (> 1 ms) galvanostatic	400 s	400 s	400 s
Interval time	0.1 s	0.1 s	0.1 s
Set current	0.001 A	0.001 A	0.001 A
Records signals (> 1 ms) galvanostatic	400 s	50 s	25 s
Interval time	0.1 s	0.1 s	0.1 s
Set current	0.000 A	0.000 A	0.000 A
Records signals (> 1 ms) galvanostatic	400 s	400 s	400 s
Interval time	0.1 s	0.1 s	0.1 s
Set current	5.000×10^{-4} A	5.000×10^{-4} A	5.000×10^{-4} A
Records signals (> 1 ms) galvanostatic	400 s	50 s	25 s
Interval time	0.1 s	0.1 s	0.1 s
Set current	0.000 A	0.000 A	0.000 A
Records signals (> 1 ms) galvanostatic	400 s	400 s	400 s
Interval time	0.1 s	0.1 s	0.1 s

3.2.4 Porous electrodes measurements

Injecting a new solution

The cell can be filled with different solutions from outside with injection syringes. Before injecting a new solution, the cell has to be flushed carefully. It is first flushed with water for several times and then flushed with the new solution for several times. In this way, ions diffuse out of the pores and are flushed away by the water and new solution. Then the new solution is injected. During the whole process the applied potential alternates between 1 V and -1 V to accelerate the diffusion of ions out of the pores. If the applied currents are approximately equal, the flushing is sufficient. The used procedure in PGSTAT100 consists of this element which is repeated several times is:

Chrono amperometry (Δt > 1 ms)	
Set potential	1.000 V
Records signals (> 1 ms) potentiostatic	100 s
Interval time	1.00 s
Set potential	-1.000 V
Records signals (> 1 ms) potentiostatic	100 s
Interval time	1.00 s

Determining duration of charging and discharging steps

To do the measurements in a reproducible way, the optimal duration of the charging and discharging step has to be determined. In the charging step, the whole electrical double layer has to be formed and the potential difference across this layer has to be equal to the applied voltage. In the discharging step, the whole electrical double layer has to be discharged and all the ions have to diffuse out of the pores. If these conditions are satisfied, the measurements can be performed in a reproducible way. Searching for the optimal duration was done by applying sequentially 1 V, -1 V and 0 V and varying the time of the 0 V (discharging) step. A solution of 1 M NaCl was injected into the cell and temperature was measured with two Pt100 probes. The following procedure was entered in PGSTAT100 with the following duration of the last step (0 V): 7200 s, 10800 s, 14400 s, 21600 s, 28800 s and 36000 s.

Chrono amperometry (Δt > 1 ms)	
Set potential	1.000 V
Records signals (> 1 ms) potentiostatic	7200 s
Interval time	1.00 s
Set potential	-1.000 V
Records signals (> 1 ms) potentiostatic	7200 s
Interval time	1.00 s
Set potential	0.000 V
Records signals (> 1 ms) potentiostatic	7200 s
Interval time	1.00 s

In the next experiment, a duration of 4 hours per step was tested. The 1 M NaCl solution was used again and temperature was measured with two Pt100 probes. The following procedure was applied:

Chrono amperometry (Δt > 1 ms)	
Set potential	1.000 V
Records signals (> 1 ms) potentiostatic	14400 s
Interval time	1.00 s
Set potential	-1.000 V
Records signals (> 1 ms) potentiostatic	14400 s
Interval time	1.00 s
Set potential	0.000 V
Records signals (> 1 ms) potentiostatic	14400 s
Interval time	1.00 s
Set potential	1.000 V
Records signals (> 1 ms) potentiostatic	14400 s
Interval time	1.00 s
Set potential	-1.000 V
Records signals (> 1 ms) potentiostatic	14400 s
Interval time	1.00 s

Set potential	0.000 V
Records signals (> 1 ms) potentiostatic	14400 s
Interval time	1.00 s
Set potential	1.000 V
Records signals (> 1 ms) potentiostatic	14400 s
Interval time	1.00 s

Measuring entropic and Joule heat effects

With steps of four hours for charging and discharging, the heat effects were measured. A 1 M NaCl solution was injected into the cell and two Pt100 temperature probes are used. The electrodes are charged to a certain voltage and then discharged to 0 V. This was repeated at different voltages. The procedure in PGSTAT100 was as follows:

Chrono amperometry (Δt > 1 ms)	Serie 1	Serie 2	Serie 3
Set potential	1.000 V	1.000 V	1.000 V
Records signals (> 1 ms) potentiostatic	14400 s	14400 s	14400 s
Interval time	1.00 s	1.00 s	1.00 s
Set potential	0.000 V	0.000 V	0.000 V
Records signals (> 1 ms) potentiostatic	14400 s	14400 s	14400 s
Interval time	1.00 s	1.00 s	1.00 s
Set potential	0.900 V	0.900 V	0.900 V
Records signals (> 1 ms) potentiostatic	14400 s	14400 s	14400 s
Interval time	1.00 s	1.00 s	1.00 s
Set potential	0.000 V	0.000 V	0.000 V
Records signals (> 1 ms) potentiostatic	14400 s	14400 s	14400 s
Interval time	1.00 s	1.00 s	1.00 s
Set potential	0.800 V	0.800 V	0.800 V
Records signals (> 1 ms) potentiostatic	14400 s	14400 s	14400 s
Interval time	1.00 s	1.00 s	1.00 s
Set potential	0.000 V	0.000 V	0.000 V
Records signals (> 1 ms) potentiostatic	14400 s	14400 s	14400 s
Interval time	1.00 s	1.00 s	1.00 s
Set potential	0.600 V	0.700 V	0.700 V
Records signals (> 1 ms) potentiostatic	14400 s	14400 s	14400 s
Interval time	1.00 s	1.00 s	1.00 s
Set potential	0.000 V	0.000 V	0.000 V
Records signals (> 1 ms) potentiostatic	14400 s	14400 s	14400 s
Interval time	1.00 s	1.00 s	1.00 s
Set potential	0.400 V	0.600 V	0.600 V

Records signals (> 1 ms) potentiostatic	14400 s	14400 s	14400 s
Interval time	1.00 s	1.00 s	1.00 s
Set potential	0.000 V	0.000 V	0.000 V
Records signals (> 1 ms) potentiostatic	14400 s	14400 s	14400 s
Interval time	1.00 s	1.00 s	1.00 s
Set potential		0.400 V	0.400 V
Records signals (> 1 ms) potentiostatic		14400 s	14400 s
Interval time		1.00 s	1.00 s
Set potential		0.000 V	0.000 V
Records signals (> 1 ms) potentiostatic		14400 s	14400 s
Interval time		1.00 s	1.00 s
Set potential		0.200 V	0.200 V
Records signals (> 1 ms) potentiostatic		14400 s	14400 s
Interval time		1.00 s	1.00 s
Set potential		0.000 V	0.000 V
Records signals (> 1 ms) potentiostatic		14400 s	14400 s
Interval time		1.00 s	1.00 s

4. Results

4.1 Pre-research

4.1.1 Temperature dependence of charging and discharging steps with constant current

In this experiment, at different temperatures a constant current was applied (50 mA) to the electrodes and potential was measured. The potential curves were shifted in a way that these curves started at 0 V and the increase was the same as the original curves. These curves can be seen in Figure 11. Potential decrease upon increasing temperature and the charging process was the same. Charge was obtained by integrating current over time.

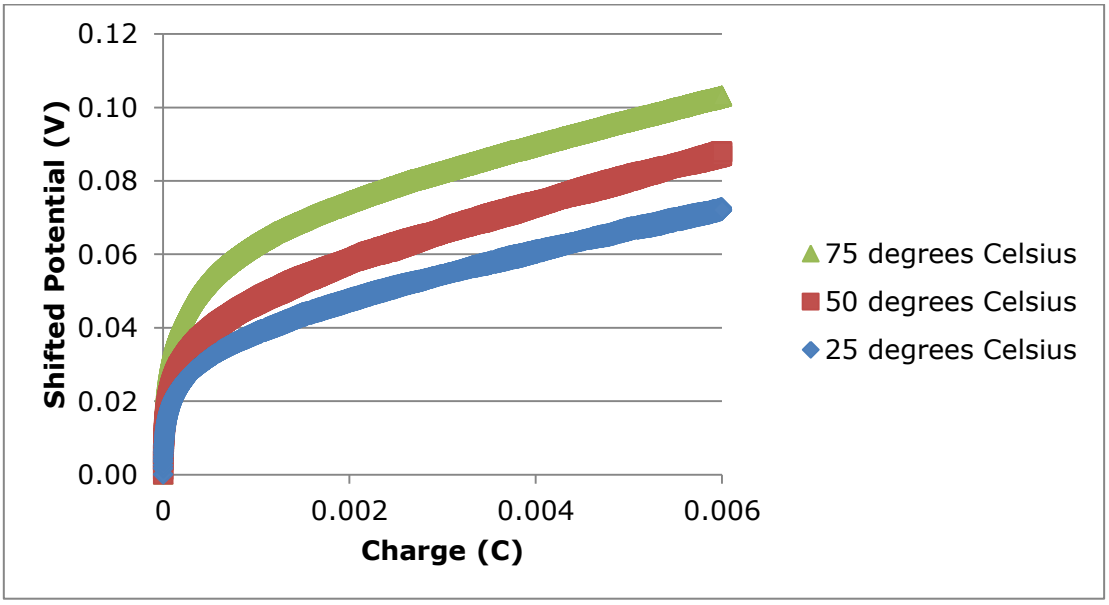

Figure 11. Shifted potential curves at different temperatures versus charge on the electrodes

These results are contrary to the theoretical predictions; at the same charge potential should increase upon increasing temperatures [2]. An increase in potential of approximately 30 mV should occur between the potentials at 25 and 50 ˚C and 50 and 75 ˚C [2]. However, the potential decreases with approximately 20 mV when the temperature was increased. Therefore, the experiments are often repeated, but the results remained the same. This remarkable contradiction can be explained with leakage current. Leakage current is a measure for the rate of charge leakage in supercapacitors [19]. The charging of capacitors is not completely efficient, a small part of the current leaks away due to imperfections and impurities in the electrodes. In electrical double layer capacitors, ions in the electrical double layer leak away. This leakage current depends on temperature: the mobility of ions increase upon increasing temperature so the leakage current is higher at higher temperatures [19]. This explains the results from the constant current study: a bigger part of the current leaks away so less charge remains to charge the capacitor (and raise the potential). This was tested experimentally by applying a voltage and measuring the current for a long time (to reach the leakage current). The leakage was two times higher at a temperature of 70 ˚C compared to room temperature.

Another problem of constant current charging is the self-discharge. Self-discharge is the leakage of charge in an open circuit after charging. The decrease in potential after the charging of the

electrodes is shown in Figure 12. A rapid decrease in potential occurs at a short time scale and a slow decrease occurs at a long time scale. This pattern can be explained with the two processes during charging of electrodes: the formation of an electrical double layer and the accumulation of an excess of ions near the surface [19]. After the charging of electrodes, the self-discharge of the double layer is relatively slow, but the excess of ions rapidly diffuses away. The typical pattern for a combination of these processes is a rapid decrease in potential at a short time scale due to the loss of excess ions and a slow decrease at a long time scale due to deformation of the double layer [19]. This pattern was observed during the constant current experiments, as can be seen in Figure 12. So the two processes might be an explanation for the self-discharge pattern. However, that has to be verified and is beyond the scope of this project. In conclusion, there is a fast self-discharge and this is an disadvantage of charging with constant current.

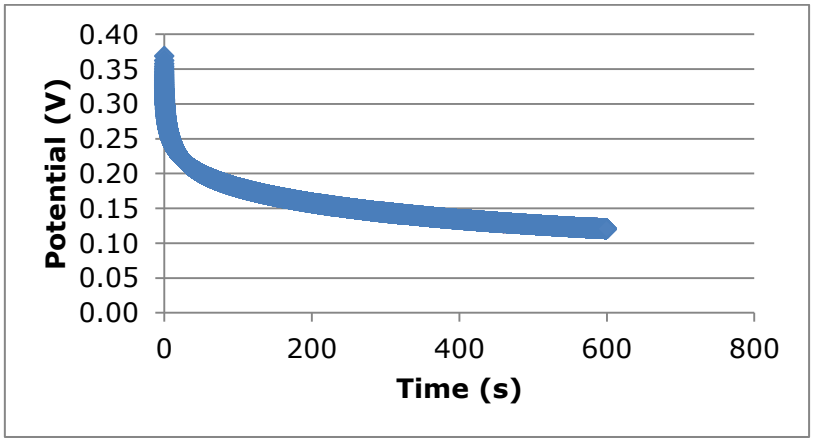

Figure 12. The decrease of the potential over time due to self-discharge after charging with constant current.

4.1.2 Temperature dependence of charging and discharging steps with constant voltage

In this experiment, the electrodes were charged with a constant voltage and thus the current semi-exponentially decreases to zero. This has the advantage that an equilibrium situation is obtained at the end of the charging step. A disadvantage is that the electrical double layer potential is unknown; only the applied potential can be measured. These experiments were performed at different temperatures and results were obtained which were in agreement with the theoretical predictions [2]. At a temperature of 67 ˚C, less charge caused a higher potential compared to room temperature. In other words, the potential increase per unity of charge was higher at higher temperatures. These experiments are reproduced and similar results are obtained.

Table 2. Overview of the voltage change per amount of charge at different temperatures.

Temperature (˚C)	ΔV (V)	Q (C)	dV/dQ
25	0.140	0.0600	2.335
67	0.152	0.0593	2.561

Moreover, the self-discharge differed from the self-discharge after constant current experiments. This is shown in Figure 13. The self-discharge curves were shifted in a way that they start at the same potential. The rapid self-discharge at the short time scale was missing and the self-discharge is much

slower than the self-discharge with constant current charging. This means that the formed electrical double layer is stable and that an equilibrium situation is obtained at the end of the charging step.

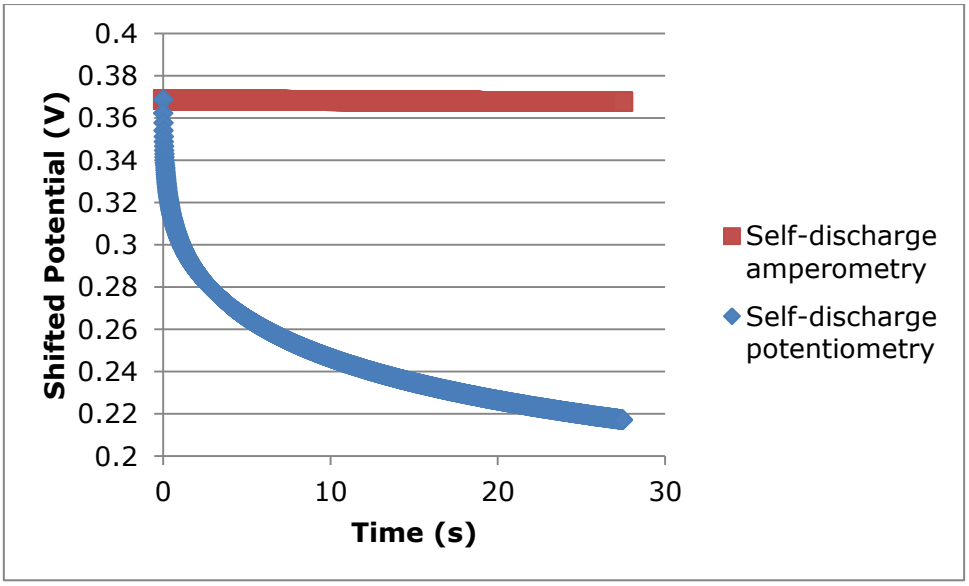

Figure 13. Shifted potential decrease over time due to self-discharge. Curves are shown after charging at constant current and constant voltage

4.1.3 Effective surface area of porous carbon electrodes

To determine the effective surface area of the porous electrodes, the capacitance of the electrodes and graphite foil was measured. The capacitance was determined as the reciprocal slope of the linear regime of a plot of charge and potential. This is shown in Figure 14 for graphite foil. The capacitance per m^2 was 83.5 F/m^2 for graphite and 2.47 x 10^3 F/m^2 for porous electrodes. The extra capacitance of porous electrodes is due to the extra surface in the pores (28.56 m^2 compared to 1 m^2 graphite surface) of activated carbon. For electrodes with 48 mm^2 surface, this represents an extra surface of 1.37 x 10^3 mm^2. The pore volume of the electrodes (with a porosity of 65 % [11]) is 10.4 mm^3. By dividing the pore volume by the pore surface, the pore size can be estimated. The thus experimentally determined pore size is 7.59 µm. The precise calculation can be found in Appendix C.

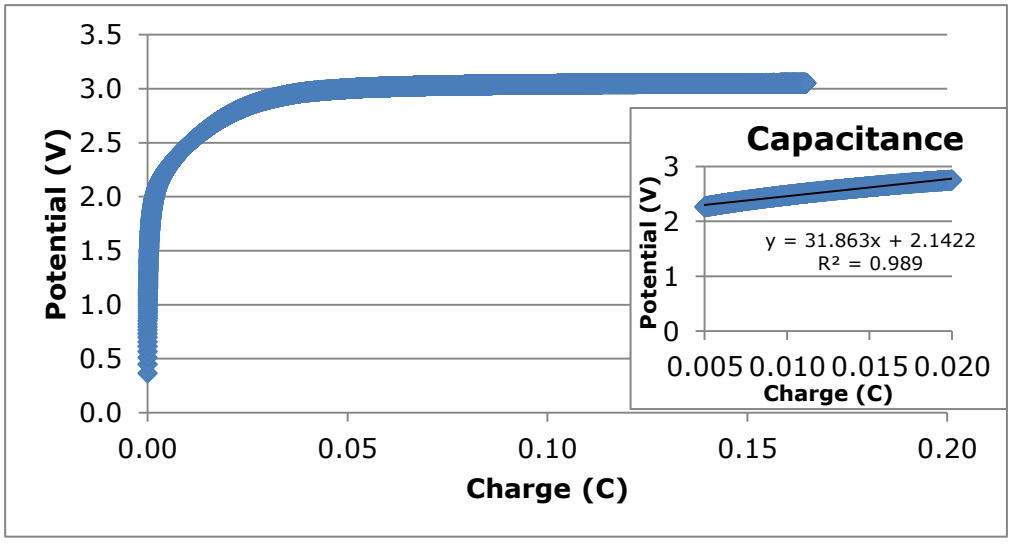

Figure 14. Plot of potential versus charge for the charging of graphite foil. Reciprocal slope of the linear part of the curve is equal to the capacitance.

The value of the effective surface can be compared to the known BET-area of this porous carbon (1330 m^2/g). With a density of 0.58 g/mL and a volume of 16 mm^3, the BET-area should be 12.3 m^2. This is much more than experimentally determined effective surface area of 1.37 x 10^3 mm^2. This huge difference states that only a small fraction of the surface area is useful for electrical double layer formation. This is supported by the high value of the pore size at the micrometer scale instead of the usual nanometer scale. Typical capacitances of porous electrodes are 500-2000 F/m^2 [12] which are in agreement with the experimentally determined capacitances. However, the method to determine the capacitance can be changed to be more accurate. Results from the cell measurements show different capacitances (corrected for different area of the electrodes) and are more reproducible. In these results the capacitance is determined by charging with constant voltages which is more reliable than charging with constant current. The capacitance of graphite can be determined in the same way and thus a more accurate estimation of the effective surface area and pore size can be obtained.

4.2 Cell measurements

4.2.1 Calibration

By current flow through resistance wire controlled amounts of Joule heating were used to calibrate the cell. Temperature effects due to Joule heating were measured and in this way the calibration was performed. In a temperature controlled system, temperature is described by

$$\frac{d\Delta T}{dt} = \frac{IV}{C} - k\Delta T \qquad (9)$$

in which $\Delta T = T - T_0$ (T_0 is the temperature of the baseline, the temperature without applied currents or voltages) , I is the current, V the potential, C the heat capacity of the cell filled with air/water and k the time constant. The term kΔT is added due to the temperature control of the system: without heat production temperature decreases exponentially with a certain time constant $k=1/\tau$ and during heat production the temperature finds an equilibrium with the temperature of the thermostat bath. At first, this formula is tested.

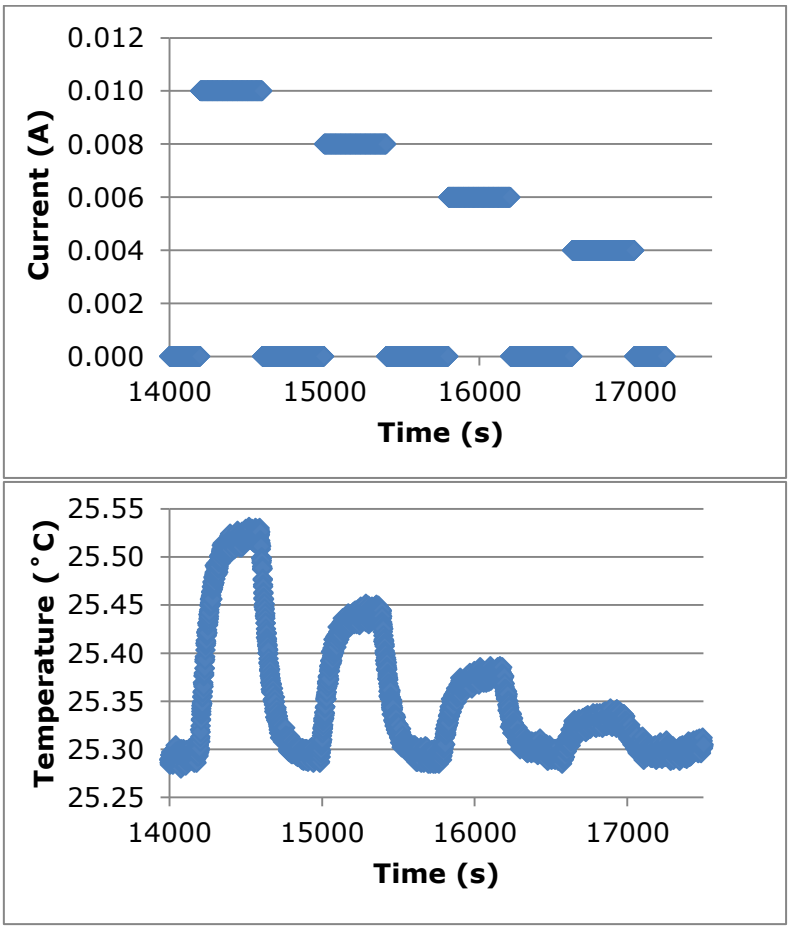

Figure 15. (Above) Overview of the different currents over time. (Below) Temperature peaks due to current during the calibration.

The currents (10, 8, 6 and 4 mA) and temperature peaks for the cell filled with water are shown in Figure 15. All the peaks increase till a certain plateau value (slope is zero) during the current flow and

exponentially decrease to T_0 without current flow. At a plateau value, the slope of ΔT over t is zero, so Equation 9 can be rewritten as:

$$IV = kC\Delta T \tag{10}$$

By plotting ΔT and IV, the product of k and C can be acquired. This is shown in Figure 16 and gives a value of 0.1809 $JK^{-1}s^{-1}$ for kC.

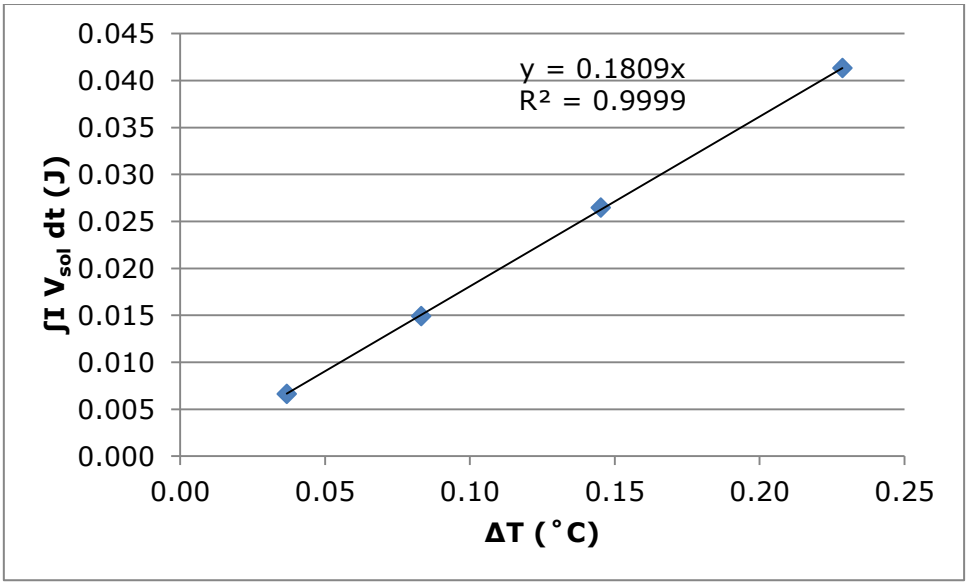

Figure 16. Plot of the integral of IV_{sol} over time versus the plateau values of the temperature peaks. Slope is equal to kC.

Moreover, from the linearity of this plot can be concluded that our formula for Δt over time works. Equation 9 can be rewritten in the following way

$$\frac{d\Delta T}{dt} = \frac{1}{C}(IV - kC\Delta T) \tag{11}$$

to simulate the experimental temperature peaks with our kC-value. C is an unknown parameter and can be estimated by using an ordinary least square method (quadratic difference between experimental and simulational data) via the Solver option in Excel. The simulations fit the experimental temperature effects very well as can be seen in Figure 17.

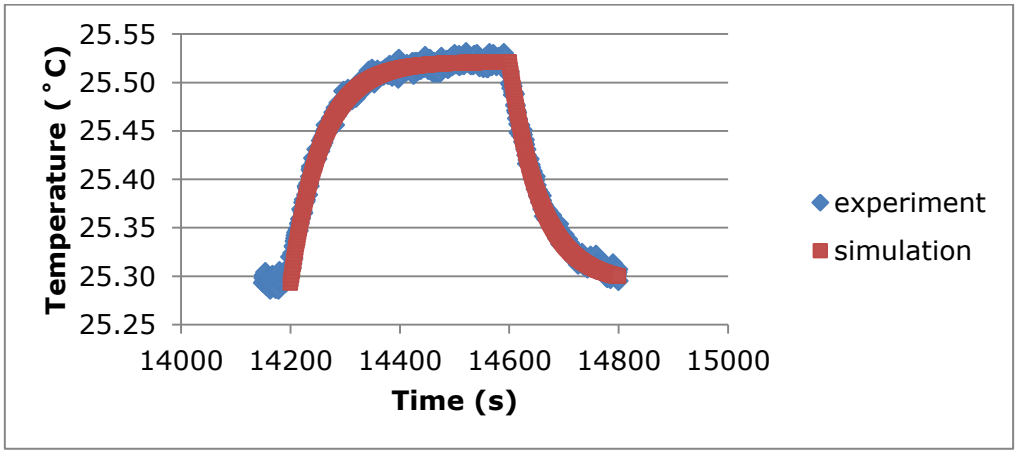

Figure 17. An experimental and simulated temperature peak (simulated with determined parameters).

By simulating the temperature curves and optimizing them with an ordinary least square method, a value for the heat capacity of 14.15 JK^{-1} is obtained for the cell filled with water. The heat capacity for the cell filled with air is determined from the slope of the first ten seconds of the temperature peaks, since the kΔT term is negligible in that part of the peaks. The slope is equal to IV/C and with known values for I and V C can be calculated. The heat capacity of the cell filled with air is 7.709 JK^{-1}. Since the heat capacity of air is negligible compared to the heat capacity of water, the difference between the capacities of the cell filled with air and water should be close to the heat capacity of water. This difference is 6.443 JK^{-1} and the heat capacity of water for the volume of the cell (approximately 1.036 mL based on the volume between the two heating elements in the cell) is 4.318 JK^{-1}. The small difference between the calculated and measured heat capacity can be explained by the extra volume of water in the connections to the injections syringes. However, this found heat capacity states that the cell measures heat effects correctly.

The only unknown parameter is k, which can be calculated by dividing kC by C. The parameters for the cell filled with water are shown in Table 3.

Table 3. Mean and standard deviation of the determined parameters of the calibration

	Mean	Standard deviation
kC	0.1809 $JK^{-1}s^{-1}$	1.37 x 10^{-3} $JK^{-1}s^{-1}$
C	14.15 JK^{-1}	3.67 JK^{-1}
k	0.01278 s^{-1}	0.0132 s^{-1}

For determining temperature effects, Equation 9 has to be integrated over time:

$$\int_{t1}^{t2} \frac{d\Delta T}{dt} dt = \int_{t1}^{t2} d\Delta T = \Delta T|_{t_1}^{t_2} \quad (12)$$

If the t_2 and t_1 are chosen in a way that at both points ΔT=0, for example at the start and the end of a temperature, the integral is zero. This brings back the previous formula

$$\int_{t1}^{t2} IV dt = kC \int_{t1}^{t2} \Delta T dt \quad (13)$$

which is very convenient. This would mean that the produced heat is equal to kC times the area of the temperature curve. In Figure 18 the calculated and measured Joule heating effects are plotted. A slope of approximately 1 is obtained (R^2=0.994) so the experimental and calculated Joule heat effects are similar. This means that heat effects can be obtained by integrating temperature peaks and multiplying with a value of kC.

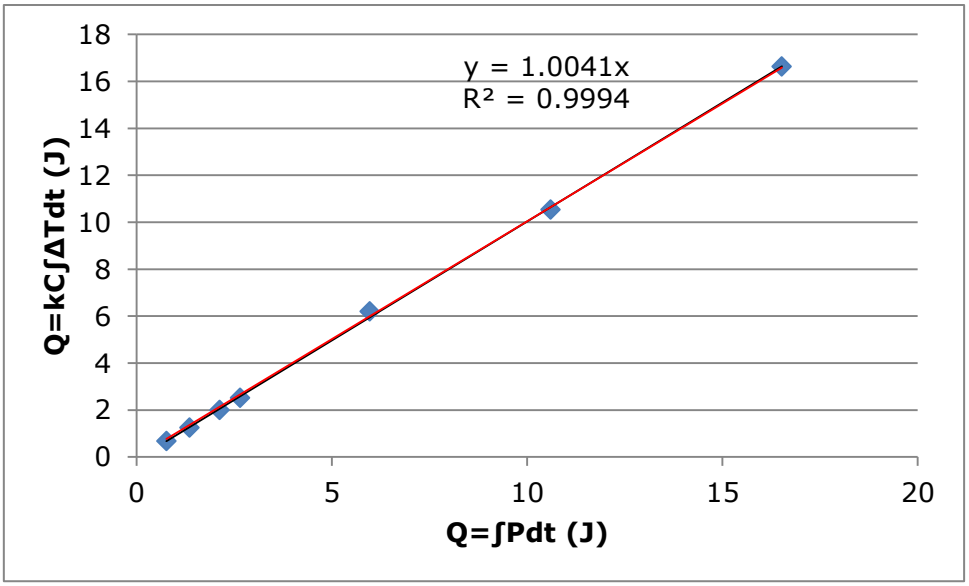

Figure 18. Experimental vs calculated Joule heating effects in a plot.

4.2.2 Determining duration of charging and discharging steps

Firstly, the optimal duration of the charging and discharging step had to be discovered. This was done by a sequence of 1 V, -1 V and 0 V (2 hours per step) and varying the 0 V discharging step. Results from this measurements (1 V and 0 V) are shown in Figure 19. The total charge is acquired by integrating the current over time.

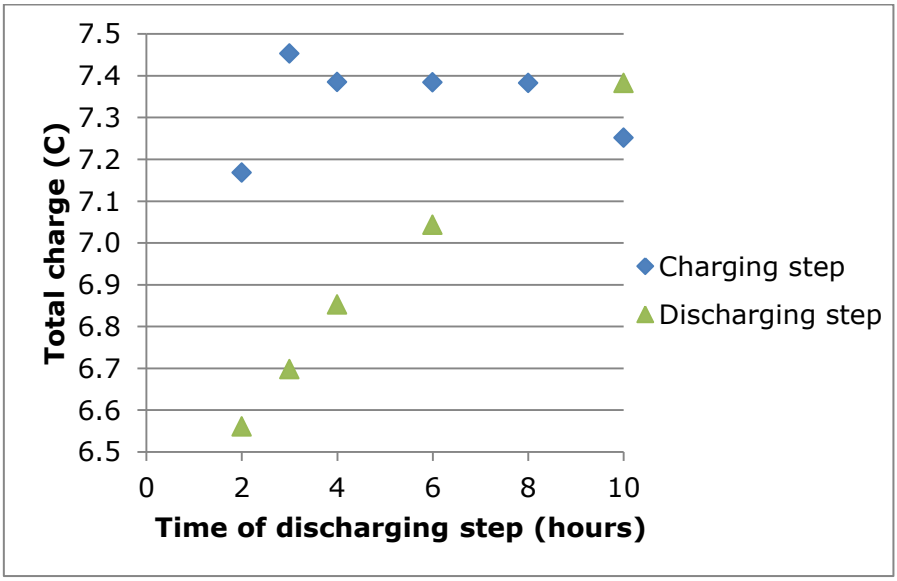

Figure 19. Total charge in charging and discharging steps as a function of the time of the discharging step.

Contrary to the discharging step, the charging step is constant after four hours (except the charging step at 10 hours discharging time). This would mean that 4 hours is enough to do reproducible charging and discharging steps. In Figure 20 the charge over time and the percentage of the total charge over time are shown for the discharging step of 10 hours. These plots again show that four hours is enough to perform the charging and discharging step.

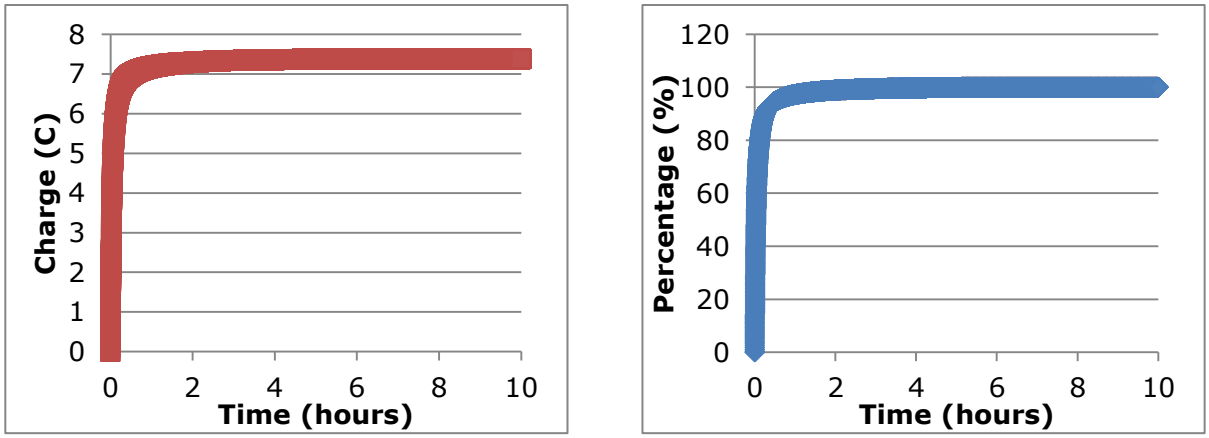

Figure 20. (Left) The amount of charge over time during the discharging step of ten hours. (Right) The percentage of the total charge (after ten hours) over time during the discharging step of ten hours.

To test this expectation the same sequence (1 V, -1 V and 0 V) with four hours per step was measured and the total charge per step was determined. Two series were done and the results are shown in Figure 21. These two series are very similar which means that four hours per step is a reproducible way to perform charging and discharging experiments.

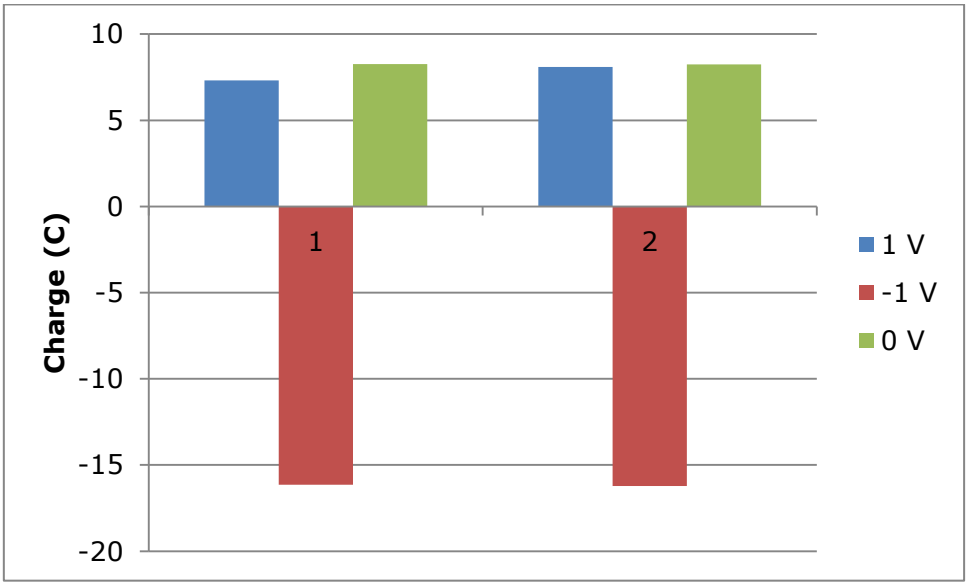

Figure 21. Diagram of the amount of charge per step for two measurements.

4.2.3 Measuring Joule and entropic heat effects

In the performed experiments the electrodes were first charged to a certain voltage and then discharged to zero volt. This was repeated at different voltages. An example of one of the results is shown in Figure 22. The current decreases semi-exponentially to zero in both steps. The first temperature peak is that from the charging step and consists of positive Joule and entropic heating. The second temperature peak is that from the discharging step and consists of positive Joule heating and negative entropic heating. To quantify the temperature peaks several corrections had to be

done. First, the temperature of the thermostat bath is averaged by taking the average of the previous and next five temperature values. Then, the average of the difference between the temperature in the cell and the average temperature in the thermostat bath is determined at a time interval without charging and discharging. Finally, ΔT is determined as follows:

$$\Delta T = T_{cell} - \bar{T}_{average\ thermostat\ bath} + \overline{(\bar{T}_{average\ thermostat\ bath} - T_{cell})} \qquad (14)$$

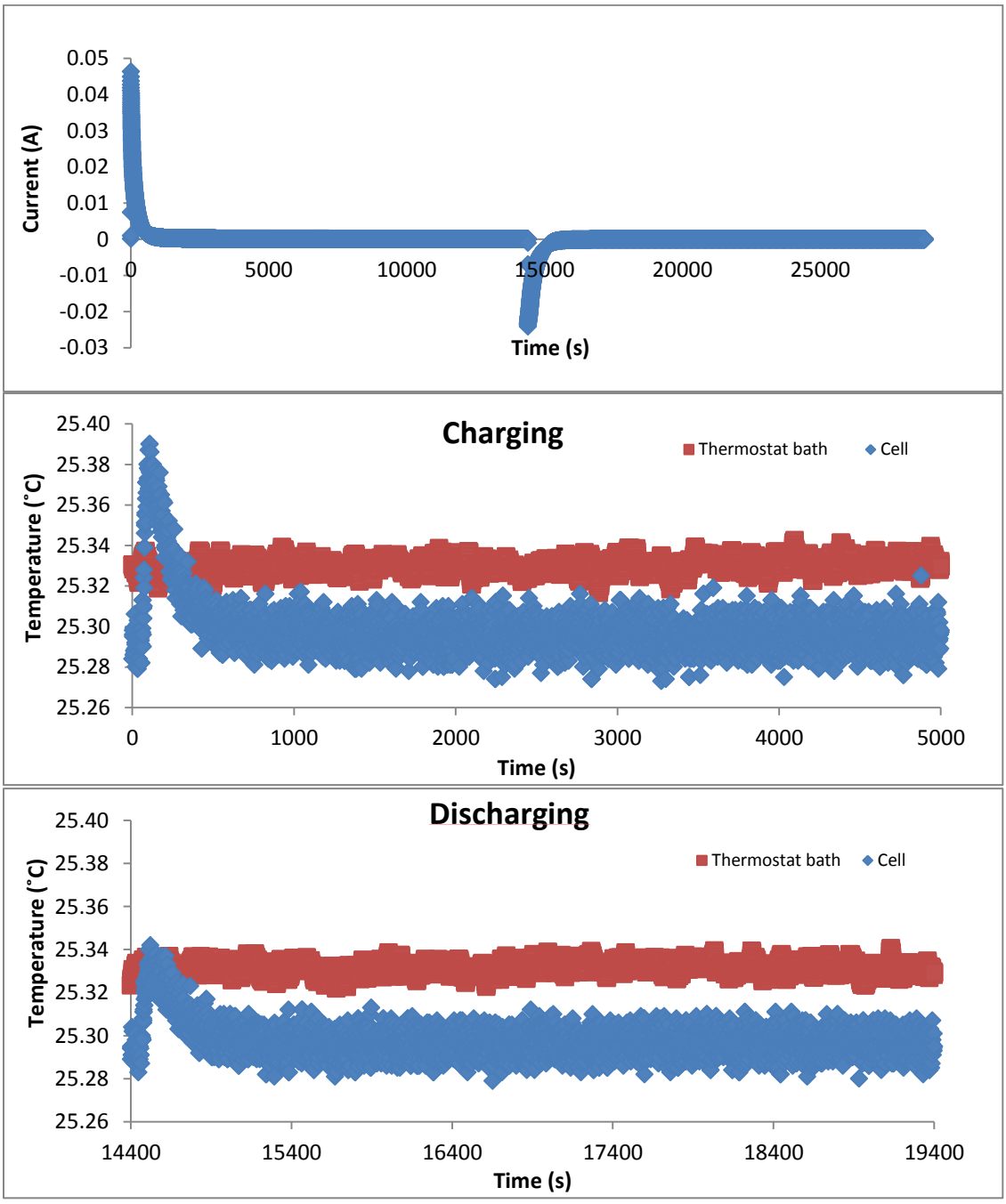

Figure 22. (Above) Current over time for a charging and discharging step. (Mid) Temperature peak during charging step. (Below) Temperature peak during discharging step.

The area of ΔT over t can be integrated to get the total heat effect. This integration was done for the first 3000 seconds of the measurements for each peak. In this measurements are two types of heating, so Equation 9 is rewritten as:

$$\frac{d\Delta T}{dt} = \frac{P_{ions}+IV_{sol}}{C} - k\Delta T = \frac{P_{total}}{C} - k\Delta T \quad (15)$$

The heat effects are given by:

$$Q_{total} = \int_{t1}^{t2} P_{total} dt = kC \int_{t1}^{t2} \Delta T dt \quad (16)$$

A value of kC is needed and the value of the calibration is not useful, because heating elements and porous carbon electrodes are totally different. However, a value of kC can be acquired in another way. The entropic heating is reversible: it is the same in the charging and discharging step but the sign is different. Joule heating depends on the amount of current and is irreversible. If the two steps are added, the sum is as follows:

$$Q_{charging} + Q_{discharging} = (Q_{Joule(+)} + Q_{entropic}) + (Q_{Joule(-)} - Q_{entropic}) = Q_{Joule(+)} + Q_{Joule(-)}$$

So by adding both steps, only Joule heating remains. Joule heating can be calculated, so the sum of both steps can both be calculated and measured experimentally. The total heat is described by

$$Q_{total} = \int_{t1}^{t2} IV_{sol} dt = kC \int_{t1}^{t2} \Delta T dt \quad (17)$$

which means that the slope of a plot of the calculated Joule effects versus the area of the temperature peaks is equal to kC. Expressions for V_{sol} are described with Equation 7 and 8. Three measurements are performed and give different kC-values which are shown in figure 23. Firstly, excluding the measurement of 10 June, the values of kC are internal consistent. However, the values decrease in time which can be due to bubble formation. The time constant does not depend much on air or water in the cell, but the heat capacity does. If the cell is filled with more air, the heat capacity of the system becomes lower. So bubble formation is in agreement with the decrease of the heat capacity. This disturbs measurements and consequently less higher temperature effects occur. An explanation for the formation of bubbles is the bad wetting of water on carbon. Evaporation is accelerated by bad wetting so gasses arise in the pores [16].

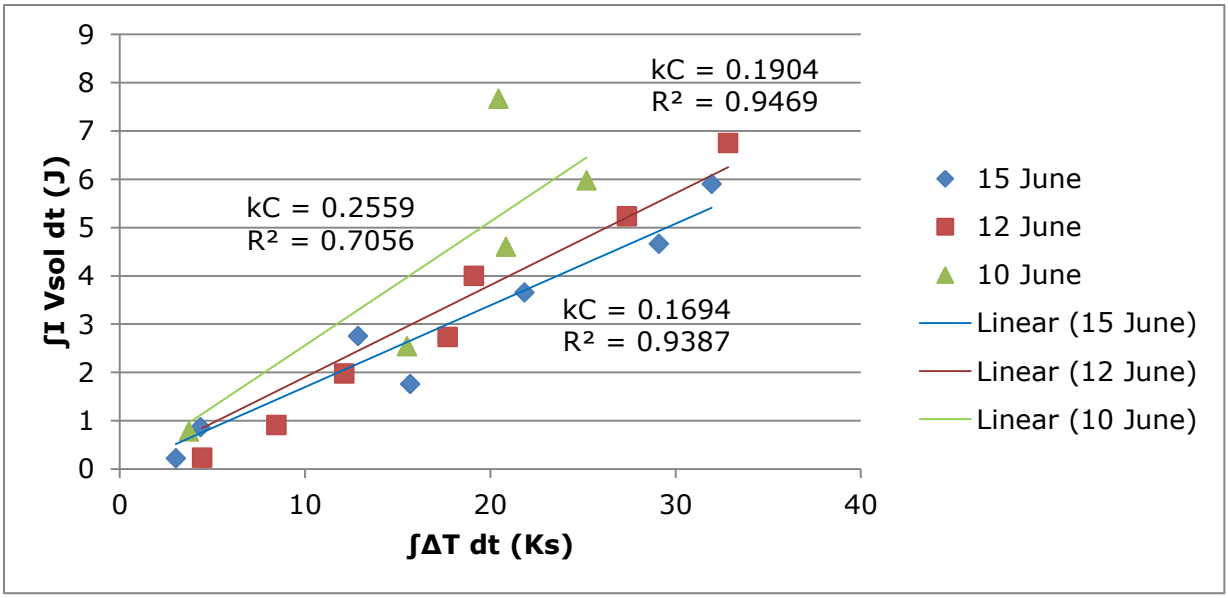

Figure 23. Plots of the calculated Joule heating versus the area of the temperature peaks for the sum of the charging and discharging step. Values of kC decrease over time.

In addition, the capacitance of the performed measurements can be determined. This was done with a plot of $V_{applied}$ versus Q: the slope is equal to the capacitance. The capacitances of the different measurements are shown in Figure 24. Knowing the dimensions of the electrodes (and the pore surface area), the capacitance per m^2 can be calculated which is approximately 246 F/m^2. This is somewhat lower than the literature value of 500- 2000 F/m^2 [12], but still a reliable capacitance. However, the capacitance, similar to the kC-value, decreases in time. This would mean that less charge is needed to reach the same voltage. An explanation is again bubble formation: this disturbs the measurements. If pores are filled partly with gas, the formation of an electrical double layer by absorbing ions is disturbed. However, to investigate why bubble formation might influence the charging process is beyond the scope of this research.

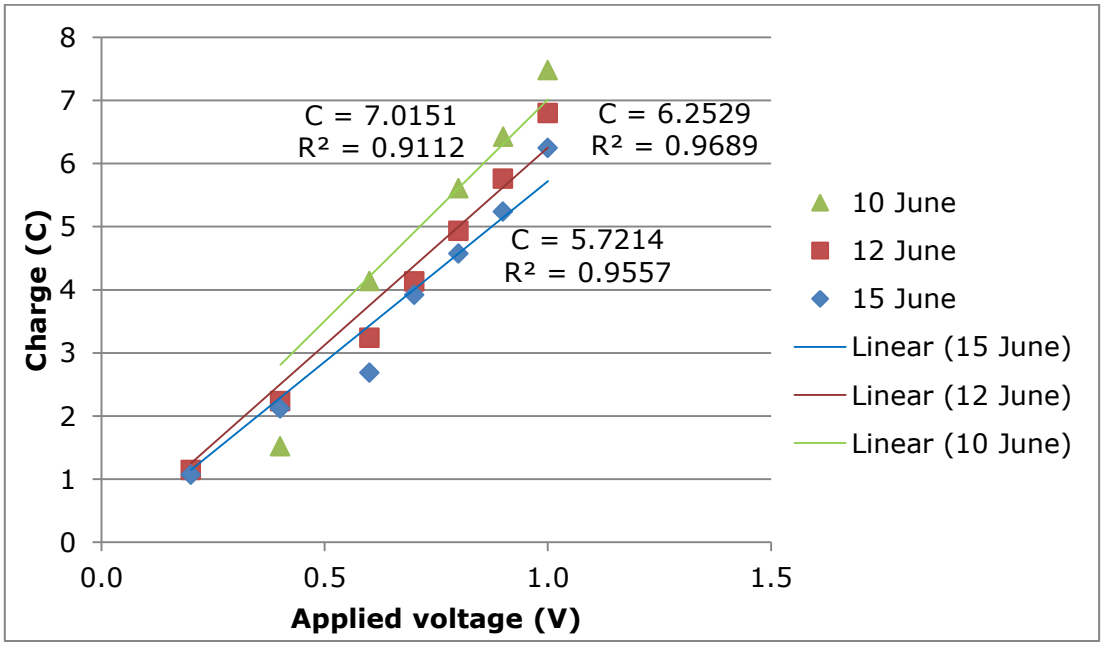

Figure 24. Plots of charge versus applied voltage in which the slope is equal to the capacitance. The capacitance decreases over time.

Nevertheless, the values of kC are known. Using them, the heat effects can be extracted out of the performed experiments. The average effects are shown in Figure 25 with standard deviations as error bars. The total heat effects are acquired by integrating the temperature peaks and multiplying with kC. The Joule heat effects are calculated by integrating IV_{sol} over time. The entropic heat effects are acquired by subtracting the Joule heat effects from the total heat effects.

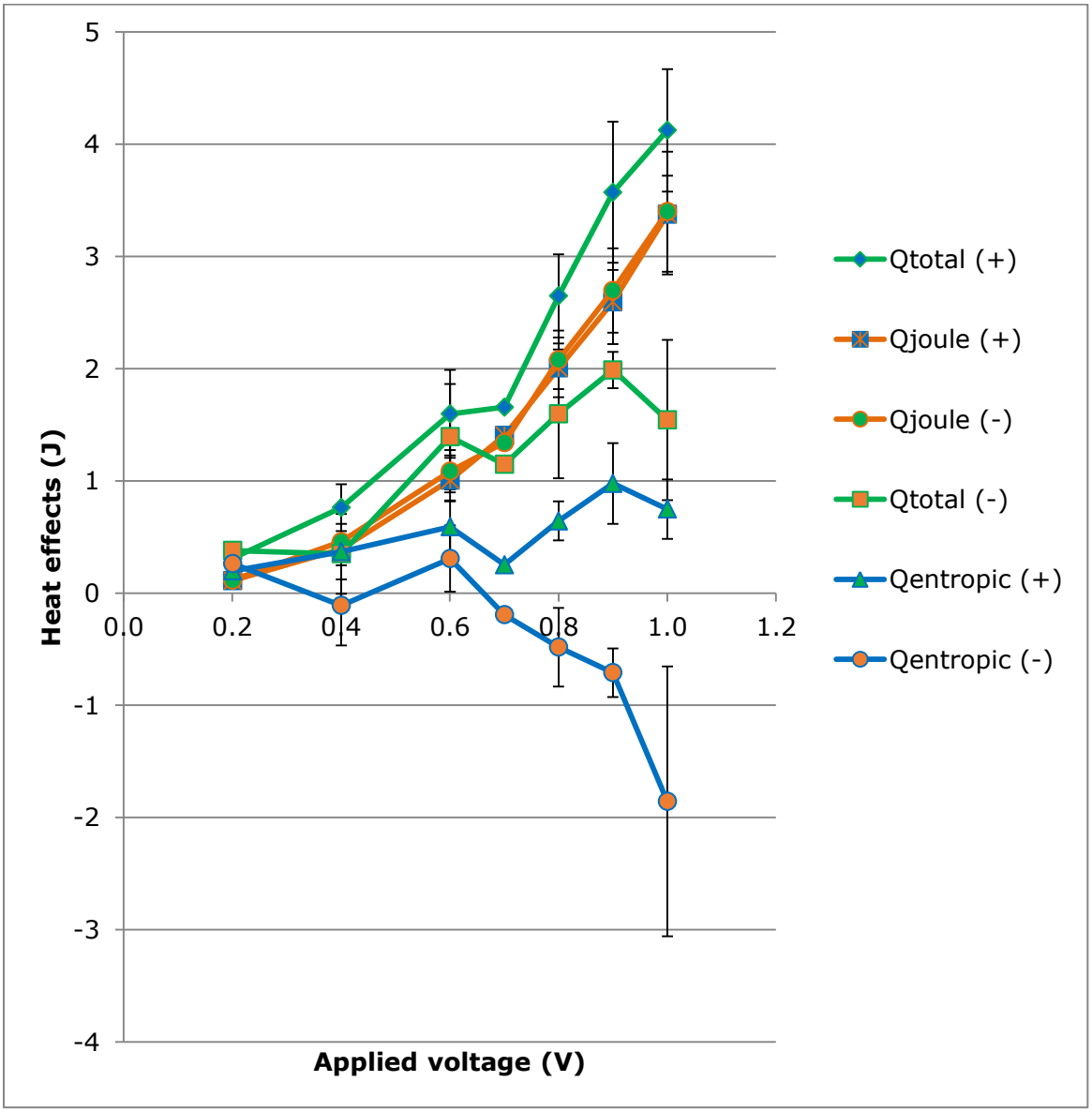

Figure 25. Total, Joule and entropic heat effects at different voltages. Error bars are standard deviations.

The total heat effects in the charging step are significantly higher than the total heat effects in the discharging step. This total heat effect consists of Joule heating and entropic heat effects. These effects can be separated. The calculated Joule effects of the charging and discharging step are very similar. This has the advantage that the differences between the total heat of charging and discharging are solely due to the entropic heat effects. These entropic heat effects are particularly positive in the charging step and negative in the discharging step. This is in agreement with theoretical predictions [2] and means that entropic heat effects upon charging and discharging really exist.

Interesting is the high value of the Joule heating steps. Joule heating can also be calculated by the integral of I^2R over time. This resistance consists of the resistance of the pores and the solution. An calculated estimation of the resistance is 107 Ω. This is a remarkably high value because the resistance of the solution is of the order of 1 Ω. So the pore resistance is very high.

At high voltages the heat effects are separable and in agreement with theory. However, at lower voltages (< 0.6 V) the effects overlap and the values of the different effects are similar. These effects are less reliable and accurate compared to higher voltages. This can be due to the noise in the temperature measurements. At lower voltages the temperature effects are smaller and more difficult to distinguish from the noise. This can be an explanation for the values that disagree with theoretical predictions.

Finally, the standard deviations of the total and entropic heat effects are high. This means that the heat effects fluctuate among the different measurements. The measurements are reproducible but the range can be diminished. The fluctuations can be explained by the bubble formation during the measurements. This disturbs the accuracy of the measurements. If this bubble formation is prevented, the fluctuations will probably decrease.

4.2.4 Comparing experimental entropic effects to theoretical predictions

The measured entropic effects can be compared to the theoretical predictions about the entropic effects [2]. The theoretical effects are converted from Kelvin to Joule. Theoretical and experimental entropic heat effects are shown in Figure 26. An extensive calculation can be found in Appendix D.

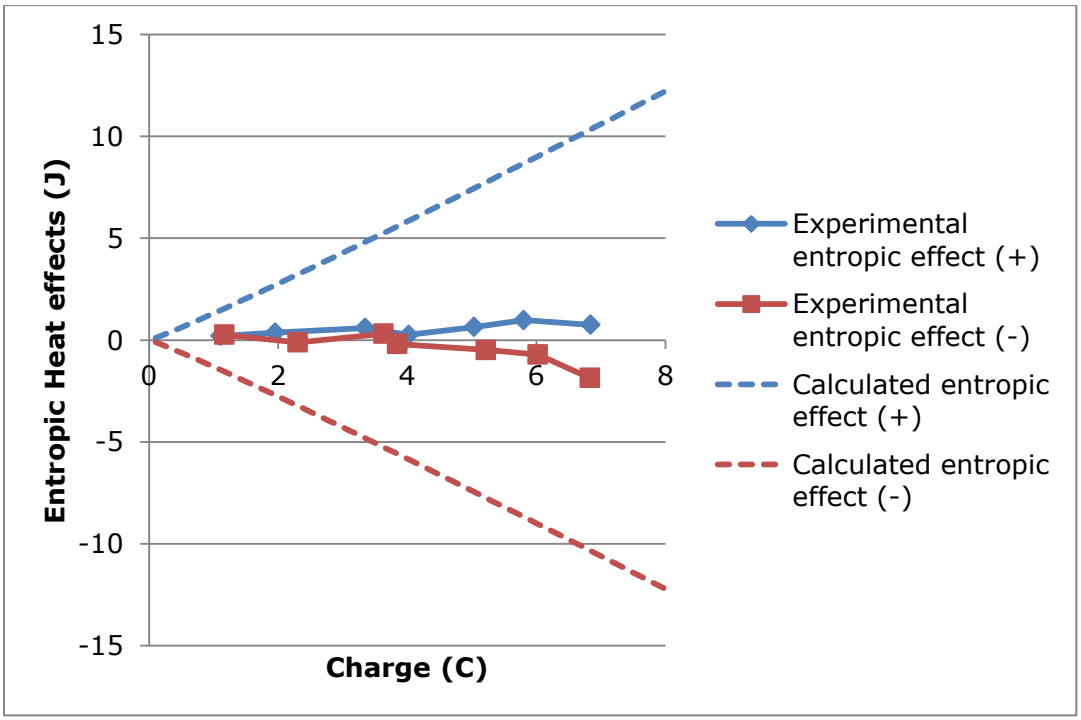

Figure 26. Experimental entropic heat effects at different charges (solid lines) and theoretical entropic heat effects [2] (dashed lines) of the charging and discharging step

The experimental effects are approximately ten times weaker than the calculated ones. An explanation for this difference might be an assumption in the theoretical predictions. For the calculation of the entropic effects is assumed that the volume of the electrical double layer is equal to the pore volume [2]. However, the electrical double layer thickness is on the order of the Debye length [15], which is approximately 0.3 nm for a 1 M NaCl solution [16]. With a pore size of 7.59 µm this assumption is not realistic. Only a small fraction of the electrical double layer is used for electrical double layer formation. This is a difference between the theoretical predictions and the experiments. A possible explanation for difference between theoretical and experimental temperature effects due to changes in ion entropy is the calibration. In our temperature controlled system heat leaks away due to heat conduction of carbon and graphite and water in the soft silicone tubes. However, this was corrected in the calibration. The calibration was performed with controlled amounts of heat production: with the calculated heat and experimental temperature peaks the system was calibrated. This is the right calibration to compare experimental heat effects to theoretical predicted ones. For the comparison of temperature effect, a calibration with controlled amount of temperature increases and decreases would be better.

Another calculation for the entropic heat effect is based on the Boltzmann entropy. The entropy of a system with all the ions in the electrical double layer is compared to the entropy with the ions randomly distributed over the whole pore volume. The Boltzmann entropy is rewritten and from with this entropy the heat effects can be described as follows [3]

$$Q_{entropic} = \frac{2kTQ}{e}\ln\left(\frac{V_{EDL}}{V_{total}}\right) \tag{18}$$

in which k is the Boltzmann constant, T the temperature, Q the charge, e the positive elementary charge, V_{total} the pore volume and V_{EDL} the volume of the electrical double layer. The volume of the electrical double layer is calculated by multiplying the pore surface (total surface without outer surface of electrodes) with the Debye length of 0.3 nm. The precise derivation and calculation of these predicted effects is given in Appendix E. A comparison of the experimental effects and calculations via this formula is shown in Figure 27.

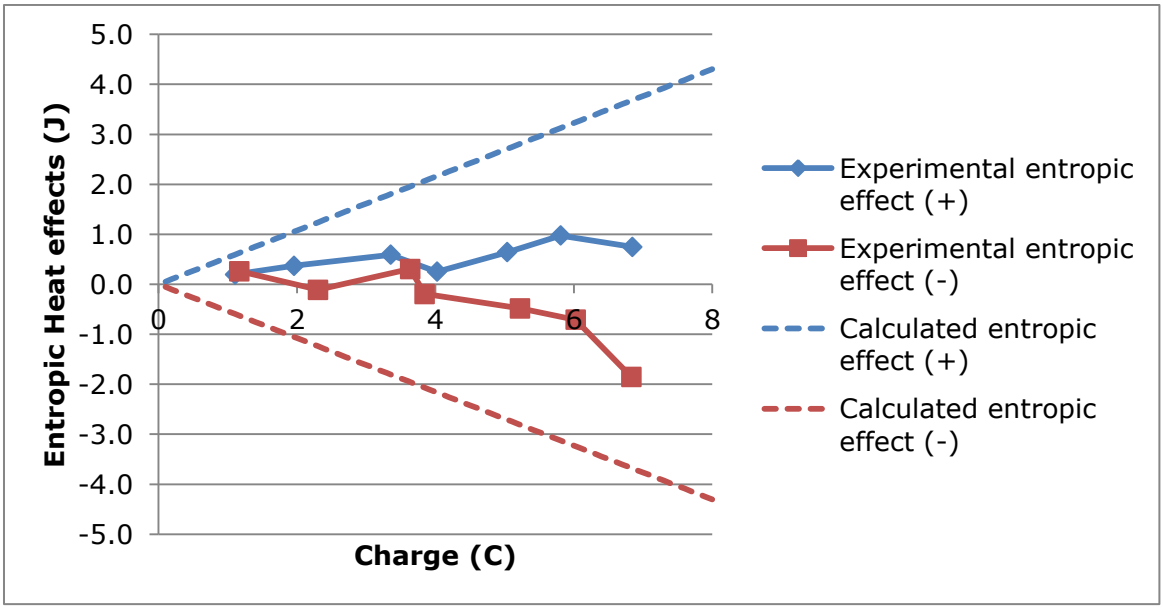

Figure 27. Experimental entropic heat effects at different charges (solid lines) and theoretical entropic heat effects [3] (dashed lines) of the charging and discharging step.

Although the calculated and experimental entropic effects are not in perfect agreement, the calculations fit the experimental data much better than the previous calculations and they have the same order of magnitude. This can be explained by the fact that the volume of the double layer is described differently. This formula is not based on the assumption that the whole pore volume consists of double layers. In this formula, the double layer thickness is estimated more precisely which might be an explanation for the better agreement between experiment and theory.

5. Conclusions

The objective of this research was to measure entropic heat effects upon charging and discharging of porous electrodes and to compare these effects to the theoretical prediction. At first, the system was successfully calibrated with controlled amounts of Joule heating. Heating elements with a fixed resistance were used: the current flow through these heating elements produced Joule heating. Afterwards, the heat effects upon charging and discharging of porous carbon electrodes were measured by applying voltages to the electrodes.

It was possible to measure the heat effects with the used setup. The temperature increase was 0.1 °C at most, but still measurable. The total heat effects were measured as temperature peaks, the Joule heat effects were calculated by integrating the product of I and V_{sol} over time and the entropic effects were acquired from the difference between the total and the Joule heat effects. The entropic heat effects and the Joule heat effects were separable, since the Joule heat effects were approximately similar for the charging and discharging step. Moreover, entropic heat effects really existed and were measurable using this setup. The effects are on the order of 1 Joule at high voltages, 0.98 Joule at 0.9 volt for example.

Entropic heat effects are positive in charging steps and negative in discharging steps and reversible according to the theoretical prediction [2]. These predictions were verified in the experiments. The size of the effects was predicted at approximately 6 K or 9 Joule at high voltages, but in experiments 0.8 K or 1 Joule was found. A possible explanation is the unrealistic assumption that the whole pore volume is equal to the electrical double layer volume [2]. A typical electrical double layer thickness of 1 M NaCl solution is 0.3 nm and the experimentally obtained pore size is 7.59 µm so the pore volume is not completely filled with electrical double layers. An alternative calculation which is based on Boltzmann entropy do take this electrical double layer volume in account [3]. Results of this calculation are in closer agreement with the experimental entropic heat effects.

In contrast to the heat effects at high voltages, those at lower voltages are less reliable. This can be due to the noise of the temperature measurement. Smaller heat effects are more difficult to distinguish from the noise and this influences the results. Another problem is bubble formation. During the measurements, bubbles are formed and these disturb the measurement. This has a big influence on the quality of the found entropic heat effects. Nevertheless, entropic heat effects are measurable in a reproducible way with this setup which is a big step in research on ion entropy in blue energy.

6. Outlook

The predicted entropic temperature effects exists and can be measured in a reproducible way. However, still much work on these entropic effects. To improve the results, measurements can be repeated and the temperature effects can be averaged to decrease the noise. Moreover, bubble formation disturbs the measurements but can be prevented. If the solutions are cleaned in an ultrasonic bath before injection into the cell, less bubble formation occurs. So bubble formation can be prevented and consequently the quality of the results enhances. Finally, the experimental method to obtain the effective surface area of porous carbon electrodes can be improved. A better value can be acquired if the cell setup is used. The capacitance of electrodes in the cell has already been determined; if the same procedure is used for graphite foil a better estimation of the effective surface area will be obtained.

The research on entropic heat effects can also be expanded. Now we only explored the heat effects at different voltages (which means different charges) in a 1 M NaCl solution. However, in blue energy devices electrodes are charged in salt water and discharged in river water [1]. For practical implementations of this entropy effects in upscaled devices, it is interesting what the influence is of different electrolyte concentrations on these effects. Moreover, thermodynamic behaviour of ions during charging and discharging is of fundamental interest. Also temperature has an influence on entropic heat effects. By measuring the entropic heat effects at different temperatures, this influence can be explored with experiments. Finally, theoretical work on the thermodynamics of ion entropy in electrical double layers can be done, for example on the influence of electrolyte concentration and temperature. Combined with experiments, this can deliver new insights and stimulates research in this field of blue energy.

7. Acknowledgements

At first, I want to thank Ben Erné for supervising me. He often helped me with advices for problems and unexpected results of experiments, he constructed the right setup and experiments to measure the temperature effects and gave me the confidence to do this research. Moreover, I want to thank him for doing this out of the box research project at the Physical and Colloid Chemistry group. I also want to thank René van Roij for the possibility to verify his theoretical prediction. I was wondering if he had an experimental project in the field of blue energy and he came up with this. I enjoyed this project and this interdisciplinary research would not be possible without his idea. Then I want to thank Maarten Biesheuvel (researcher at Wageningen University and Wetsus, a blue energy research institute) for useful discussions about experiments and about the setup for the capacitive mixing method. He also gave us activated carbon as a present which was very useful. I want to thank Pieter-Bart Peters for collaborating in the research and corresponding with Doriano Brogioli for experimental details. For two months, we did experimental research together every Tuesday afternoon. I want to thank the glassblowers for engineering the beautiful cell in which we did the measurements. Then I want to thank FCC for doing my research here. I have been at the research group for almost half a year and this was a pleasant stay. Finally I want to thank my parents, brother and friends for the distraction and the support during this bachelorthesis. A combination of work and distraction is healthy and pleasant.

8. References

[1] Brogioli, D. (2009). Extracting Renewable Energy from a Salinity Difference Using a Capacitor. *Physical Review Letters, 103 (058501),* 1-4.

[2] Janssen, M., Härtel, A., & Van Roij, R. (2014). Boosting capacitive blue-energy and desalination devices with waste heat. *Physical review letters*, *113*(26), 268501.

[3] Schiffer, J., Linzen, D., & Sauer, D. U. (2006). Heat generation in double layer capacitors. *Journal of Power Sources*, *160*(1), 765-772.

[4] Norman, R.S. (1974). Water salination: A source of energy. *Science*, *186*, 350–352.

[5] Semiat, R. (2008). Energy issues in desalination processes. *Environmental science & technology*, *42*(22), 8193-8201.

[6] Kraaijvanger, C. (2014). Nederland opent 's werelds eerste blauwe energiecentrale [news article]. Downloaded at 17 July 2015 from http://www.scientias.nl/s-werelds-eerste-blauwe-energiecentrale-opent-op-de-afsluitdijk/

[7] Rica, R. A., Ziano, R., Salerno, D., Mantegazza, F., van Roij, R., & Brogioli, D. (2013). Capacitive mixing for harvesting the free energy of solutions at different concentrations. *Entropy*, *15*(4), 1388-1407.

[8] Logan, B. E., & Elimelech, M. (2012). Membrane-based processes for sustainable power generation using water. *Nature*, *488*(7411), 313-319.

[9] Anderson, M. A., Cudero, A. L., & Palma, J. (2010). Capacitive deionization as an electrochemical means of saving energy and delivering clean water. Comparison to present desalination practices: Will it compete?. *Electrochimica Acta*, *55*(12), 3845-3856

[10] Boon, N., & Van Roij, R. (2011). 'Blue energy' from ion adsorption and electrode charging in sea and river water. *Molecular Physics, 109,* 1229-1241.

[11] Brogioli, D., Zhao, R., & Biesheuvel, P.M. (2011). A prototype cell for extracting energy from a water salinity difference by means of double layer expansion in nanoporous carbon electrodes. *Energy & Environmental Science, 4,* 772-777.

[12] Simon, P., & Gogotsi, Y. (2008). Materials for electrochemical capacitors. *Nature materials*, *7*(11), 845-854.

[13] Gouy, M. (1910). Sur la constitution de la charge électrique à la surface d'un électrolyte. *Journal de Physique Théorique et Appliquée, 9*, 457-468.

[14] Chapman, D. L. (1913). A contribution to the theory of electrocapillarity. *Philosophical Magazine, 25*, 475-481.

[15] Schmickler, W., & Santos, E. (2010). *Interfacial electrochemistry*. New York: Springer Science & Business Media.

[16] Ball, D. (2003). Physical Chemistry. Stamford: Cengage Learning

[17] Dietrich, T. (2001). UltraCaps - A new Energy Storage Device for Peak Power Applications [lecture]. *18th Electric Vehicle Symposium*, Berlin, Germany

[18] Kötz, R., Hahn, M., & Gallay, R. (2006). Temperature behavior and impedance fundamentals of supercapacitors. *Journal of Power Sources*, *154*(2), 550-555.

[19] Ricketts, B. W., & Ton-That, C. (2000). Self-discharge of carbon-based supercapacitors with organic electrolytes. *Journal of Power Sources*, *89*(1), 64-69.

[20] Conway, B. E., Birss, V., & Wojtowicz, J. (1997). The role and utilization of pseudocapacitance for energy storage by supercapacitors. *Journal of Power Sources*, *66*(1), 1-14.

[21] Flores-Rivera, C. F. (2012). Modeling and Behavior Analysis of a Membraneless Fuel Cell. *ISRN Applied Mathematics*, *2012*.

[22] Thermocouples, how they work [internet article]. Downloaded at 17 July from http://www.sensorland.com/HowPage017.html

9. Appendices

A Derivation of quantitative expression for the temperature effect

The expression for the temperature effect is derived from the condition that the entropy is constant [2]:

$$dS\ (Q,T) = 0 \quad \text{A.1}$$

This can be rewritten as follows:

$$(\frac{\partial S}{\partial Q})_T dQ + (\frac{\partial S}{\partial T})_Q dT = 0 \quad \text{A.2}$$

$$dT = -(\frac{\partial T}{\partial S})_Q (\frac{\partial S}{\partial Q})_T dQ \quad \text{A.3}$$

Now these fractions must be substituted for experimental parameters. This can be done with the following equations:

$$V_{EDL} = \frac{AL}{2} \quad \text{A.4}$$

$$C_Q = c_Q V_{EDL} = c_Q \frac{AL}{2} \quad \text{A.5}$$

$$(\frac{\partial T}{\partial S})_Q = \frac{T}{C_Q} = \frac{2T}{c_Q AL} \quad \text{A.6}$$

$$dQ = eAd\sigma \quad \text{A.7}$$

If A.6 and A.7 are substituted in A.3, the following equation is obtained

$$dT = -\frac{2T}{C_Q L}(\frac{\partial S}{\partial Q})_T ed\sigma \quad \text{A.8}$$

A Maxwell relation is used to substitute the last fraction (A.10 into A.8) to get A.11:

$$dF = -TdS + \varphi d\sigma \quad \text{A.9}$$

$$(\frac{\partial \varphi}{\partial T})_Q = -(\frac{\partial S}{\partial Q})_T \quad \text{A.10}$$

$$dT = -\frac{2T}{C_Q L}(\frac{\partial S}{\partial Q})_T ed\sigma = \frac{2T}{C_Q L}(\frac{\partial \varphi}{\partial T})_Q ed\sigma \quad \text{A.11}$$

B. Specifications of the cell used for temperature controlled measurements

The cell consists of three precisely engineered glass plates which are separated by teflon spacers. A schematic drawing of the first glass plate is shown in Figure 28:

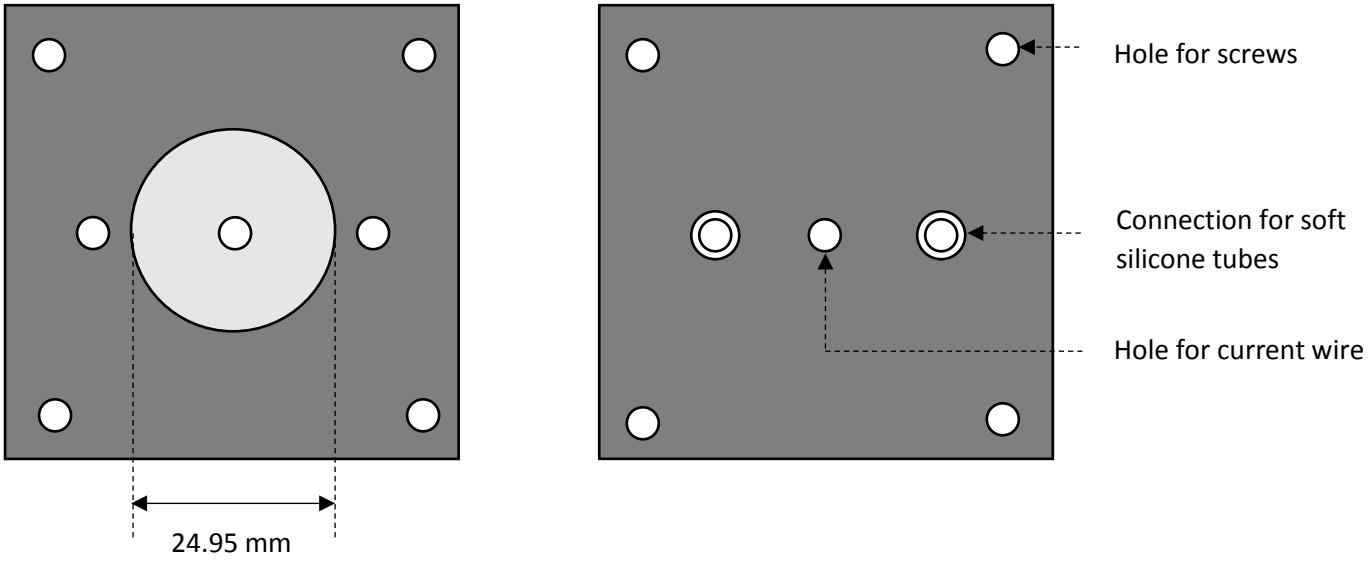

Figure 28. Schematic drawing of the first glass plate of the cell. (Left) Front side of this glass plate with a circular cavity for electrodes and heating elements. (Right) Backside of the glass plate with two connections for soft silicone tubes.

On the front side of this glass plate is a circular cavity with a diameter of 24.95 mm in which an electrode or heating element can be placed. In this cavity is a hole for the connection of the electrode/heating element with current wires. Screws are placed in other four holes to compress the cell. On the backside are two connections for the soft silicone tubes which are connected to injection syringes outside the thermostat bath. In this way, different solutions can be injected into the cell.

A schematic drawing of the second glass plate is shown in Figure 29:

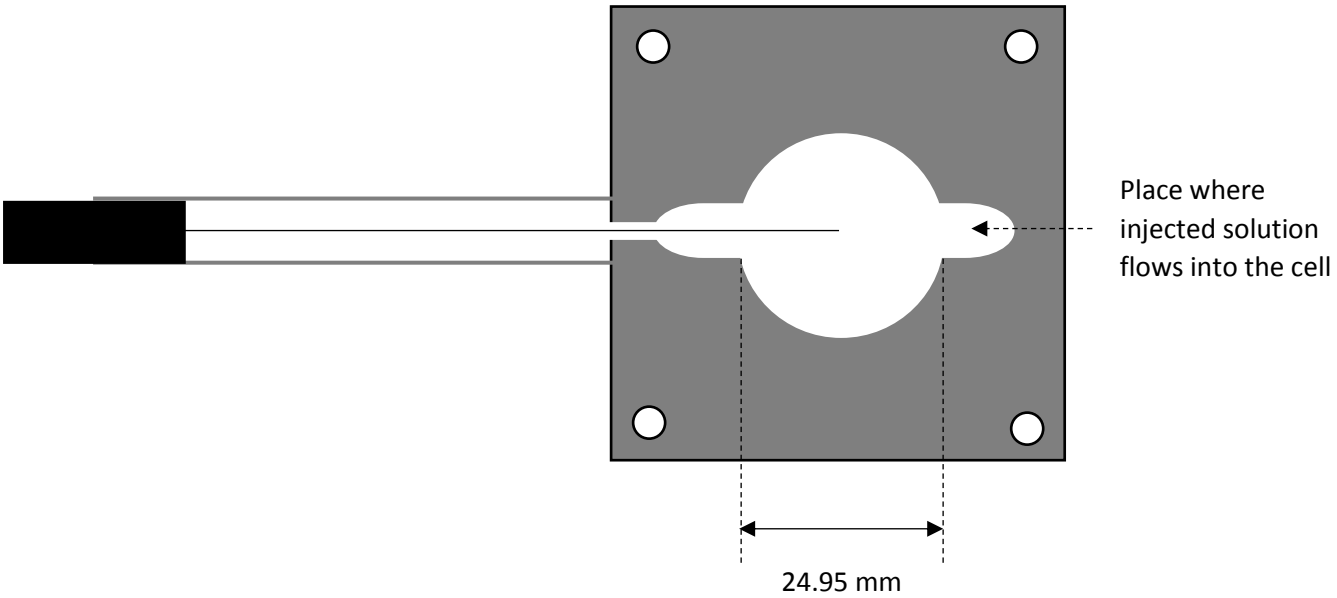

Figure 29. Schematic drawing of the second glass plate of the cell. In the middle is a big hole for the solution between the electrodes and for a temperature probe to measure the temperature effects.

In the middle of the cell is a hole with the same size of the electrodes and at the same height of the electrodes. Above and beneath this circular hole are the places were the injected solution comes into and out of the cell. In the middle of the cell is a temperature probe. The probe is circumvented by a glass tube which comes out of the cell.

The last glass plate is similar to the first, but the connections for the soft silicone tubes are missing. It is shown in Figure 30:

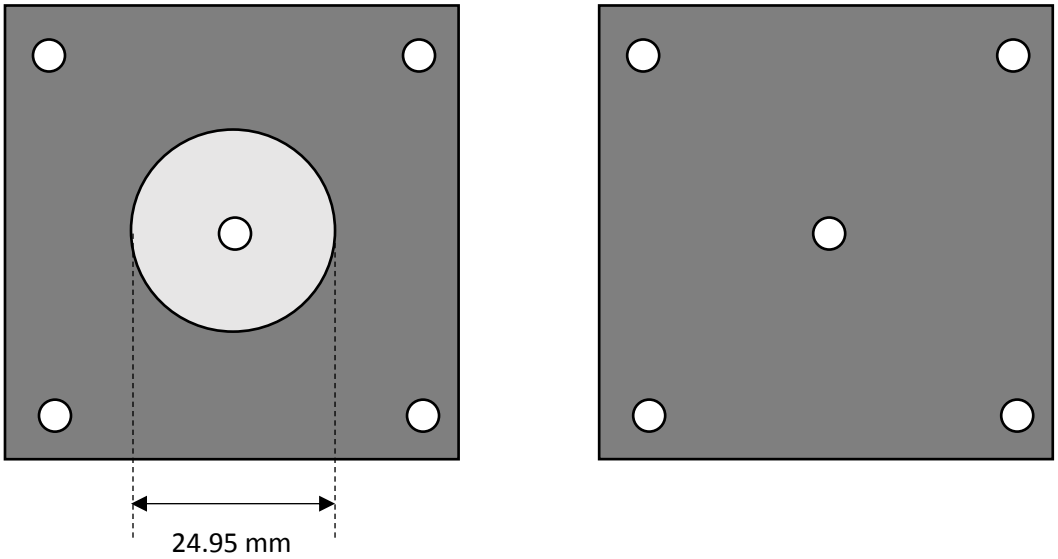

Figure 30. Schematic drawing of the third glass plate of the cell. In the middle is a circular cavity for an electrode or heating element

These three glass plates are compressed with plastic screws. Between the glass plates are teflon spacer with a hole at the same size and height of the electrode/heating element. The function of the spacer is to prevent the solution to flow out of the cell. The tube in which the temperature probe is placed is fixed in the lid. This lid is placed on the thermostat bath which completes the setup.

C. Calculation of the effective surface area and pore size of porous carbon electrodes

The effective surface area can be calculated with the capacitance of porous carbon and (non-porous) graphite. The measured capacitance were 0.0259 F for graphite (309.6 mm^2) and 0.119 F for carbon (48 mm^2). The capacitance (F) per m^2 was 83.54 for graphite and 2469 for carbon.

Assuming that all the surface of graphite is used for electrical double layer formation, the difference with carbon is only due to the surface area of the pores of carbon. So the total surface of porous carbon becomes:

$$\frac{2469}{83.54} = 29.56\ m^2$$

This surface area consists of an outer surface area of 1 m^2 and a pore surface area of 28,56 m^2. The outer surface area of the electrodes is 48 mm^2, so the total surface area becomes:

$$48\ mm^2 \times \frac{2469\ C/m^2}{83.54\ C/m^2} = 1419\ mm^2$$

The extra surface is the total surface (1419 mm^2) minus the outer surface (48 mm^2) which is 1371 mm^2.

With a density of 0.58 g/cm^3 and the electrode volume of 16 mm^3, the weight of the electrodes is 9.28 x 10^{-3} g. The literature value of the BET-area is 1330 m^2/g, so the BET-area of the electrodes is 12.3 m^2 which is much more than the experimentally found value of 1419 mm^2.

The pore size is the quotient of the pore volume and the pore surface. The pore surface is equal to the extra surface and is 1371 mm^2 for the electrodes. The pore volume is the volume of the electrodes (16 mm^3) multiplied with the porosity (65 %). This becomes 10.4 mm^3. The pore size is:

$$\frac{10.4\ mm^3}{1371\ mm^2} = 7.59 \times 10^{-3} mm = 7.59\ \mu m$$

D. Calculation of entropic heat effects

The entropic temperature effects can be calculated with [2]:

$$dT = -\frac{2T}{C_Q L}\left(\frac{\partial S}{\partial Q}\right)_T e d\sigma = \frac{2T}{C_Q L}\left(\frac{\partial \varphi}{\partial T}\right)_Q e d\sigma \quad \text{D.1}$$

However, the results are in Joule units, so the formula has to be converted from temperature to heat effects with:

$$dq = CdT = c_Q V dT \quad \text{D.2}$$

First, D.3 is substituted in D.1, which gives D.4

$$dQ = eAd\sigma \rightarrow \frac{dQ}{A} = ed\sigma \quad \text{D.3}$$

$$dT = \frac{2T}{C_Q L}\left(\frac{\partial \varphi}{\partial T}\right)_Q e d\sigma = \frac{2T}{C_Q L}\left(\frac{\partial \varphi}{\partial T}\right)_Q \frac{dQ}{A} = \frac{2T}{C_Q V}\left(\frac{\partial \varphi}{\partial T}\right)_Q dQ \quad \text{D.4}$$

This expression for the temperature effect can be converted to heat effects with D.2:

$$dq = 2T\left(\frac{\partial \varphi}{\partial T}\right)_Q dQ \quad \text{D.5}$$

This is an convenient expression because charge and temperature are measured. Only the dependence of the potential on temperature has to be calculated. This can be done with D.6:

$$\psi = \frac{2k_B \mathrm{T}}{e} \sinh^{-1} \frac{\sigma}{\sqrt{8cN_A \epsilon_0 \epsilon_r k_B \mathrm{T}}} \quad \text{D.6}$$

The used parameters for this formula are shown in Table 4. The surface charge density was acquired by dividing the total charge by the surface area of the electrodes. The total charge was variable and has a range of 0 to 8 Coulomb. The potential at 298 and 299 K was calculated and the difference was used as dΨ/dT at constant charge. So at each amount of total charge, this fraction was different. By integrating D.5, the following expression for the entropic heat effects is obtained:

$$q = 2T\left(\frac{\partial \varphi}{\partial T}\right)_Q Q \quad \text{D.7}$$

These heat effects are calculated at different amount of charge (0 to 8 Coulomb) and compared to the experimental values. This is shown in Figure 26 at page 35.

Table 4. Values of parameters used for D.6. Parameters are obtained from [16]

k_B	1.38 x 10^{-23} J/K
e	1.602 x 10^{-19} C
c	0.001 mol/m^3
Na	6.02 x 10^{23} mol^{-1}
ε_0	8.85 x 10^{-12} F/m ($CV^{-1}m^{-1}$)
ε_r	67
A_{total}	3.13 x 10^{-2} m^2

E. Derivation and calculation of entropic heat effects based on Boltzmann entropy

The Boltzmann entropy depends on the probability to realize a desired state of the system in the following way [3]:

$$S = k \ln p \qquad \text{E.1}$$

Our desired state is that all the ions are in the electrical double layer. In an uncharged state, all ions are homogeneously distributed over the solution with a volume of V_{tot}. The desired state is achieved in the charged state and the electrical double layer has a volume of V_{EDL}. The probability that all the ions (N) are in the V_{EDL} is:

$$(\frac{V_{EDL}}{V_{total}})^N \qquad \text{E.2}$$

This can be substituted into E.1 and rewritten as:

$$S = k \ln(\frac{V_{EDL}}{V_{total}})^N = kN \ln(\frac{V_{EDL}}{V_{total}}) \qquad \text{E.3}$$

The amount of ions can be expressed as:

$$N = \frac{2CU}{e} = \frac{2Q}{e} \qquad \text{E.4}$$

This can be explained as follows. All ions build up a certain voltage of the electrical double layer. If this voltage is multiplied with the capacitance of the double layer, the charge in the double layer is obtained. Since every ions has a positive or negative charge ‘e’, the number is ions is equal to the quotient of Q and ‘e’. Since there are two double layers, the quotient is multiplied with two.

If E.4 is substituted in E.3, the following equation is obtained [3]:

$$S = \frac{2kQ}{e} \ln(\frac{V_{EDL}}{V_{total}}) \qquad \text{E.5}$$

This expression for the ion entropy must only be rewritten to an expression for heat. This can be done with:

$$dS = \frac{dq}{T} \qquad \text{E.6}$$

So, the entropic effect can be acquired by filling in E.6 in E.5:

$$dq = TdS = \frac{2kTdQ}{e} \ln(\frac{V_{EDL}}{V_{total}}) \qquad \text{E.5}$$

Which can be integrated into:

$$q = \frac{2kTQ}{e} \ln(\frac{V_{EDL}}{V_{total}}) \qquad \text{E.5}$$

With this expression, the heat effects can be calculated. But first expressions for both volumes are necessary. The total volume is the pore volume in this case. A part of this pore volume functions as electrical double layer volume. The electrical double layer is equal to the Debye length, which is approximately 0.3 nm for 1 M NaCl [15]. If this thickness is multiplied with the pore surface area, the volume of the electrical double layer is obtained. The values of these and other parameters are shown in Table 5. The charge varies from 0 to 8 Coulomb in this calculation. Results of the calculation are shown in Figure 27 at page 36.

Table 5. Values of parameters used for E.5. Parameters are obtained from [16]

k_B	1,38 x 10^{-23} J/K
e	1.602 x 10^{-19} C
V_{total}= V_{pore}	319.068 mm^3
A_{pore}	3.03 x 10^{-4} mm^2
κ^{-1}	0.3 x 10^{-6} mm
V_{EDL}	9.08 x 10^{-3} mm^3